Chlorophyll *a* fluorescence induction kinetics in leaves predicted from a model describing each discrete step of excitation energy and electron transfer associated with Photosystem II

Xin-Guang Zhu[1], Govindjee[2], Neil Baker[3], Eric de Sturler[4], Donald R. Ort[5], Stephen P. Long[1]

1. Department of Plant Biology and Crop Sciences, University of Illinois at Urbana Champaign, 379 Madigan Laboratory, 1201 W. Gregory Drive, Urbana, IL, 61801
2. Department of Plant Biology and Department of Biochemistry, 265 Morrill Hall, 505 S Goodwin Ave, Urbana, IL 61801 USA
3. Department of Biological Sciences, University of Essex, John Tabor Labs, Colchester, Essex CO4 3SQ England
4. Department of Computer Science, 4314 Thomas M. Siebel Center for Computer Science, University of Illinois at Urbana Champaign, IL 61801 USA
5. Department of Plant Biology, University of Illinois at Urbana Champaign, USDA/ARS, 148 Madigan Laboratory, 1201 W. Gregory Drive, Urbana, IL, 61801

Corresponding Author:
Prof. Stephen P. Long
stevel@life.uiuc.edu
Tel: 217 333 2487
FAX: 217 244-7563

ABSTRACT

Induction of chlorophyll *a* fluorescence is widely used as a probe for studying photosynthesis. On illumination, fluorescence emission rises to a maximum through a series of transients, termed O J I and P fluorescence induction curve (FI). FI kinetics reflect the overall performance of photosystem II (PSII). Although FI kinetics are commonly and easily measured, there is a lack of consensus as to what controls the characteristic series of transients, partially because most of the current models of FI focus on subsets of reactions of PSII, but not the whole. Here we present a model of fluorescence induction, which includes all discrete energy and electron transfer steps in and around photosystem II, avoiding any assumptions about what is critical to obtaining O J I P kinetics. This model successfully simulates the observed kinetics of fluorescence induction including O J I P transients. The fluorescence emission in this model was calculated directly from the amount of excited singlet-state chlorophyll in the core and peripheral antennae of PSII. Electron and energy transfer were simulated by a series of linked differential equations. A variable step numerical integration procedure (*ode15s*) from MATLAB provided an computationally efficient method of solving these linked equations. This *in silico* representation of the complete molecular system provides an experimental workbench for testing hypotheses as to the underlying mechanism controlling the O J I P kinetics and fluorescence emission at these points. Simulations based on this model showed that J corresponded to the peak concentrations of $Q_A^-Q_B$ (Q_A: the first quinone electron acceptor of photosystem II; Q_B: the second quinone electron acceptor of photosystem II) and $Q_A^-Q_B^-$ and I to the first shoulder in the increase in concentration of $Q_A^-Q_B^{2-}$. The P peak coincided with maximum concentrations of both $Q_A^-Q_B^{2-}$ and PQH_2. In addition, simulations using this model suggest that different ratios of the peripheral antenna and core antenna lead to differences in fluorescence emission at O without affecting fluorescence emission at J I and P. Increase inactive PSII center increase fluorescence emission at O phase and correspondingly decrease F_v/F_m.

KEY WORDS: photosynthesis, chlorophyll fluorescence, model, system biology, in silico

INTRODUCTION

When dark-adapted oxygenic photosynthetic cells are illuminated chlorophyll (chl) *a* fluorescence shows complex induction kinetics (FI) termed the Kautsky curve, which is characterized by a series of inflexions in the rate of rise in the fluorescence level (F) termed the OJIP transients. Each letter denotes a distinct inflexion point; i.e. a point where dF/dt = 0 in the induction curve. Chl *a* fluorescence is widely used as a probe for different aspects of photosynthesis since fluorescence measurements are non-invasive, highly sensitive, fast and easily conducted (Bolhár-Nordenkampf et al., 1989). Furthermore, FI may be measured with relatively inexpensive equipment despite the potential wealth of information generated about the primary events of photosynthesis (Govindjee, 1995, Krause & Weis, 1991, Lazar, 1999). Since FI varies under different stress conditions, e.g. high light and low temperatures, FI has been used in studying the stress physiology of photosynthesis (Baker et al., 1983, Krause & Weis, 1991, Rohacek & Bartak, 1999, Sayed, 2003).

Fluorescence induction (FI) kinetics reflect the overall performance of photosystem II (PSII) following dark adaptation. Although FI kinetics are commonly and easily measured, there is a lack of consensus as to the underlying mechanisms controlling the characteristic series of transients, perhaps in part because previous models of FI do not include all of the processes involved in excitation energy transduction and photochemistry by PSII. For example, several fluorescence models were constructed to study FI in the presence of 3-(3', 4' - dichlorphenyl) - 1,1 - dimethylurea (DCMU) or for FI in low light fluxes (Lavergne & Trissl, 1995, Vavilin et al., 1998). These models predict the performance of photosynthetic electron transfer reactions to the point of Q_A reduction. Stirbet *et al.* (1998) calculated the fluorescence emission based on the reduction state of Q_A, not directly from the amount of singlet-excited chlorophylls and the rate constants for different energy dissipation process from singlet-excited chlorophyll as in previous models. Strasser and Stirbet (2001) hypothesized that the accumulation of reduced pheophytin has a key role in FI kinetics. Schreiber and Krieger (1996) modeled variable fluorescence based on decrease in rate of primary charge

separation and increase in rate of charge recombination. This is modulated by changes in the rate constant of heat dissipation, nonradiative decay to the ground state from $P_{680}^{+}Pheo^{-}$ and spin dephasing resulting in triplet state of the radical pair. Lebedeva *et al*. (2002) developed a model which simulated FI over a range of light fluxes and incorporated the effect of membrane potentials on the rate constants of various reactions. These two models (Lebedeva et al., 2002, Schreiber & Krieger, 1996) did not however include the molecular mechanism of the oxygen evolution complex. A recent model (Lazar, 2003) provided a detailed description of reactions around PSII to simulate FI. However, neither of these models (Lazar, 2003, Lebedeva et al., 2002) included the differentiation of core and peripheral antennas in the light harvesting complex of PSII. Collectively, these models (Lazar, 2003, Lebedeva et al., 2002, Schreiber & Krieger, 1996, Stirbet & Strasser, 2001) developed explanations of the FI kinetics based on the assumption that a different single process or subset of processes determines the response.

Here we use an alternative approach, in which all of the discrete steps involved in light capture, excitation energy transfer and electron transfer associated with PSII at both the donor side and the acceptor side are included; i.e. no assumptions are made about what may be excluded for simplification. We then examine how alteration of individual steps affects the simulated FI curve. In addition to using a complete description of all the energy and electron transfer reactions, our approach describes individually the different components associated with PSII activities, rather than representing them together as intermediate complexes (see Fig. 1). The first objective of this study was to test whether such a complete model can successfully simulate the FI kinetics under normal physiological conditions, e.g. without DCMU. Secondly, this *in silico* representation of the complete system was used to test hypotheses derived from previous models underlying mechanisms controlling FI kinetics. Thirdly, the effects of changes in the rate constants of the excitation energy and electron transfer processes associated with PSII on FI are examined. Finally, the effects of different proportions of PSII inactive centers on FI were examined.

THE MODEL AND THE ASSUMPTIONS

A schematic representation of the model is shown in Fig. 1. The whole model is composed of the following major components: peripheral antenna system of PSII, core antenna system of PSII, oxygen evolving complex, PSII reaction center (P_{680} which is the primary electron donor of PSII), pheophytin (Pheo) which is the primary electron acceptor of PSII, the redox-active Tyrosine of the D_1 protein, one tightly bound plastoquinone Q_A, and one loosely bound plastoquinone Q_B. Water molecules donate electrons to P_{680}^+, while the plastoquinol pool is required to exchange with Q_BH_2 and transfer the reducing equivalent to the cytochrome b_6f complex and provide electrons for subsequent electron acceptors (Fig. 1).

The followings assumptions are used in our model and underlie the series of equations given in next section :

1) Chl *a* fluorescence (> 80%) is assumed to be emitted from PSII complexes only. Although PSI complexes are weakly fluorescent, variable fluorescence is attributed to PSII only. Antenna chlorophylls however contribute to partitioning of excitation energy (Krause & Weis, 1991).
2) The light harvesting system consists of two distinct types of pigment-protein complexes, *i.e*. the PSII core antenna system and the peripheral antenna (Horton et al., 1996). In our model, Chl *a* fluorescence is assumed to be emitted from chlorophyll molecules in both peripheral and core antenna, and excitation energy in core antenna of the closed reaction centers can migrate to the core antenna of open reaction centers with a given probability (Deprez et al., 1990, Krause & Weis, 1991, Joliot & Joliot, 1964).
3) The process of oxygen evolution is assumed to result from a succession of non-interacting oxygen-evolving complexes (OEC) with sequential redox states (Forbush et al., 1971, Kok et al., 1970). These different redox states of OEC are represented as different S states (S_n) with the subscript indicating the number of accumulated oxidizing equivalents or positive charges. When four oxidizing equivalents have been accumulated, an oxygen molecule is evolved, and the S state reset to S_0 and another cycle starts. The transition between each successive state of the oxygen evolulving

complex requires absorption of the energy of one photon: $S_0 \rightarrow S_1 \rightarrow S_2 \rightarrow S_3 \rightarrow (S_4) \rightarrow S_0 \rightarrow S_1$ … … The positive or oxidizing equivalent is obtained from P_{680}^+ via the tyrosine Z (Y_z) of the D_1 protein. This model assumes the rate constants of electron transfer reactions from OEC to Y_z^+ are the same for each S redox state. Primary charge separation occurs in the PSII reaction center, which generates P_{680}^+ and $Pheo^-$. An electron is transferred from $Pheo^-$ to the first plastoquinone electron acceptor Q_A, which in turn reduces Q_B; Q_A is bound tightly to its site while Q_B is bound loosely to its site in PSII (Velthuys & Amesz, 1974). The times for the transitions of $Q_A^-Q_B \rightarrow Q_AQ_B^-$ and $Q_A^- Q_B^- \rightarrow Q_AQ_B^{2-}$ are assumed to be 150 μs and 400 μs respectively (Bowes & Crofts, 1980).

4) After Q_B sequentially receives two electrons from Q_A^-, Q_B becomes fully reduced in the form of Q_B^{2-} which is then protonated to form Q_BH_2. For simplicity, we have assumed that protonation of Q_B^{2-} is instantaneous. Q_BH_2 exchanges with oxidized plastoquinone (PQ) in the thylakoid membrane. The oxidized plastoquinone binds to the PSII Q_B binding site and re-forms Q_B again. PQH_2 in the thylakoid membrane is oxidized through the cytchrome b_6f complex (Cyt b_6f). It is assumed, as in the model of Stirbet *et al.* (1998) that reactions beyond Cyt b_6f do not affect the fluorescence induction curve.

5) Oxidized PQ is assumed to act as a direct quencher of excitation energy in PSII and not simply as a photochemical quencher; the changes in the redox state of the PQ pool (Kramer et al., 1995, Vernotte et al., 1979) and their effects on fluorescence were included in the model.

6) A closed reaction center is defined as a PSII reaction center in which the associated Q_A is reduced. Therefore the proportion of open reaction centers (q) is given by:

$$q = [Q_A]/([Q_A]+ [Q_A^-]) \quad \ldots\ldots \quad (1)$$

The model assumes a probability parameter *p* as the likelihood of the migration of excitation energy from the core antenna of a closed reaction center to that of an open reaction center (Deprez et al., 1990, Joliot & Joliot, 1964).

7) Except where noted, all reactions in our model are described using a first order kinetic equation, *e.g.* the rate of exciton transfer from the peripheral to the core

antenna, v_{AU}, is calculated as: $[A_p]k_{AU}$, where $[A_p]$ is the concentration of excited singlet-state chlorophylls located in the peripheral antenna and k_{AU} is the rate constant of excitation energy transfer from the peripheral to the core antenna; the reversible electron transfer between Q_A and Q_B, and the oxidation of plastoquinol in the thylakoid membrane through the cytochrome b_6f complex are assumed to have first-order kinetics, as in the model of Stirbet *et al.* (1998). The only exception to first order kinetics are the reactions for exchange of plastoquinones, *e.g.* the exchange of oxidized PQ with $Q_AQ_B^{2-}$ (or $Q_AQ_BH_2$) are assumed to be second order.

8) Lebedeva et al. (2002) showed that electric field effects are of consequence to FI only in measurements in low and medium light fluxes. In this study, a saturating PPFD of 3000 □mol m^{-2} s^{-1} is used for simulation of the fluorescence induction curve; as a result, the influence of the electrical field on fluorescence emission can be ignored. Therefore, the changes in the rate constants of electron transfer from P_{680} to Q_A and from Q_A^- to Q_B upon changes in the electric field across the thylakoid membrane during a dark to light transition are not considered in this model.
9) The net charges of the OEC influence the rate constants of primary charge separation and charge recombination. However, only a minor fraction of PSII are thought to be affected (Dau, 1994), therefore the effect of different S states on rate constants of primary charge separation and charge recombination are ignored in our model. Baake & Schloder (Baake & Schloder, 1992) have shown that consideration of other reactions describing electron transfer steps beyond the oxidation of reduced PQ pool does not improve model fit to the experimentally recorded fluorescence induction curve at low light intensity, up to P on the induction curve. Therefore, only the reactions prior to PQH_2 oxidation are considered in our model.
10) Previous models (Stirbet *et al*. 1998, Lebedeva *et al*. 2002, Trissl and Lavergne 1995, Vredenberg 2000) have not accounted for the heterogeneity of PSII, i.e. the Q_B-reducing and Q_B-nonreducing PSII reaction centers, found in nature (Krause & Weis, 1991). In our model, the effects of different proportions of Q_B-nonreducing PSII reaction centers are considered. Our model assumes that the inactive centers have their own core antenna, which is 50% of size of an active reaction center, and does not contain peripheral antenna (Chylla & Whitmarsh, 1990). The inactive PSII

centers are also assumed to have their own oxygen evolution complex, Q_A and Q_B. The chlorophylls detached from core antenna and all the chlorophylls of peripheral antenna of inactive center are assumed to be separated from inactive PSII reaction center.

RATE EQUATIONS DESCRIBING EACH EXCITATION/ELECTRON TRANSFER REACTION

This section describes the rate equations representing the model structure and assumptions in the sequence of excitation energy absorption, excitation energy transfer, charge separation and electron transfer around active PSII reaction centers. Reactions around inactive PSII reaction centers use the same rate equations except that the rate constant for electron transfer beyond Q_A is assumed to be zero.

1. Light absorption by different components of the photosystems.

The amount of excitation energy incident on different components of the PSII antenna is determined by the total absorbed excitation energy, the concentration of chlorophylls in different components of PSII units, and the concentration of chlorophylls in PSI units. The PSII unit consists of more than 20 subunits (Hankamer et al., 1997), which are simplified here to one PSII reaction center, one PSII peripheral antenna and two PSII core antenna complexes (Fig. 1). The PSII peripheral antenna complex contains 220 chlorophyll *a* and *b* molecules, and the two PSII core antenna complexes contain about 35 chlorophylls each (Peter & Thornber, 1991). Therefore, it is assumed that a PSII unit contains 290 chlorophyll molecules. Similarly to the PSII unit, the PSI unit is composed of one PSI core complex with about 96 chlorophylls and one peripheral antenna binding about 80~120 chlorophylls (Chitnis, 2001). Consequently, a PSI unit contains 200 chlorophylls in our model. As stated in the assumption, the number of chlorophylls of core antenna of inactive reaction center is half of that of the active PSII reaction center, i.e. 35 chlorophylls. Assuming the ratio of inactive to active PSII reaction center is x, then the chlorophyll content associated with one active photosynthetic unit (*i.e.* one PSII and associated PSI complexes) unit is $(290 + 200n + 70x + 220x + 200nx)$, where n

represents the ratio of PSI units to PSII units where 290 represents the total number of chlorophylls in both peripheral and core antenna of active PSII, 200*n* represents the number of chlorophylls in antenna of PSI associated with one active PSII reaction center, 70*x* represents the total number of chlorophylls for core antenna of inactive PSII centers among which half of chlorophylls are detached from the core antenna, 220*x* represents the number of chlorophylls in peripheral antenna of inactive PSII centers, and 200*nx* represents the number of chlorophylls of PSI associated with inactive PSII reaction centers for one active PSII center. A default value $n = 1$ is used in the current model. Assuming the total incident photon flux density (PFD) is I_{in}, the incident PFD on peripheral antenna of active PSII will be calculated as:

$$I_a = 220 I_{in} / (290 + 200n + 70x + 220\,x + 200\,nx) \quad \ldots\ldots \quad (2)$$

Similarly, the incident photon flux density on the PSII core antenna of active PSII unit is:

$$I_c = 70 I_{in} / (290 + 200n + 70x + 220\,x + 200\,nx) \quad \ldots\ldots \quad (3)$$

The incident photon flux density on the core antenna of inactive PSII center is calculated similar to equation 3 (in Appendix II).

2. Excitation energy dissipation as heat and fluorescence

The excitation energy of excited singlet-state chlorophyll is assumed to dissipate through four different pathways: photochemistry, heat, fluorescence, and transfer to other chlorophyll molecules. The rate equations of all these four reactions were assumed to follow first-order kinetics as did by Stirbet *et al*. (1998). For example, assuming that the concentration of excited singlet-state chlorophylls in peripheral antenna is A_p, the fluorescence emission (v_{Af}) and heat dissipation (v_{Ad}) from peripheral antenna are calculated as

$$v_{Af} = [A_p]\, k^a_f; \quad \ldots\ldots \quad (4)$$

$$v_{Ad} = [A_p] k^a_d; \quad \ldots\ldots \quad (5)$$

Where $[A_p]$ is the concentration of the excited singlet-state chlorophyll in the peripheral antenna of PSII; k^a_f and k^a_d are the rate constants for heat dissipation and fluorescence emission from peripheral antenna respectively.

3. Excitation energy equilibrium and the primary charge separation reaction

The model assumes that excitation energy of chlorophylls in the core antenna reaches equilibrium instantaneously. The equilibrium between the excitation energy in the antenna chlorophyll of the PSII core complex (Chl^*P_{680}) and the excitation energy in P_{680} ($ChlP_{680}^*$) is represented as $Chl^*P_{680} \leftrightarrow ChlP_{680}^*$. The excited-state energy of different chlorophylls is estimated from the absorption spectrum by:

$$E = \frac{hc}{\lambda_{abs}} \qquad \ldots\ldots (6)$$

where h is Planck's constant, c is the speed of light, and λ_{abs} is the peak wavelength of light absorbance of certain chlorophyll in our model. An excitation equilibrium is reached when chlorophylls absorbing different wavelength stay at their excited states with a probability proportional to the Boltzmann factor $\exp[-E_i/kT]$, where E_i is the energy content of the lowest excited-state energy of chlorophyll, T is temperature and k is the Boltzmann constant. Therefore,

$$\frac{[Chl^*P_{680}]}{[ChlP_{680}^*]} = \frac{k_{-t}}{k_t} = \exp[-hc/(kT)(\lambda_{Chl}^{-1} - \lambda_P^{-1})] \qquad \ldots\ldots \quad (7)$$

where k_t is the rate constant of excitation energy transfer from Chl^*P_{680} to $ChlP_{680}^*$, and k_{-t} is the rate constant of excitation energy transfer from $ChlP_{680}^*$ to Chl^*P_{680}. λ_{Chl} and λ_P represent the wavelengths of the maximum absorbance of antenna chlorophyll (673 nm) and reaction center chlorophyll (680 nm) respectively (Schatz et al., 1988).

Equation 7 for calculating the ratio of $[Chl^*P_{680}]$ and $[ChlP_{680}^*]$ does not consider the relative concentration of P_{680} and other chlorophylls in the core antenna. If there are N chlorophylls associated with one P_{680}, the amount of excitation energy reaching P_{680} at equilibrium will decrease gradually with increase in N. Considering both a) the energy difference and b) the number of chlorophyll molecules in the PSII core antenna, the amount of P_{680}^*Pheo is calculated as:

$$[P_{680}{}^{*}\text{Pheo}] = [U]\left(1+\frac{k_{-t}}{k_t}\right)^{-1}/N \qquad \ldots\ldots \quad (8)$$

Where U represents the total excited singlet-state chlorophylls (including $P_{680}{}^{*}$) in the PSII core antenna. According to Eqn 10, changes in *N* will lead to changes in the concentration of $P_{680}{}^{*}$Pheo, which will inevitably increase the rate of primary charge separation. This has been confirmed by measurements of the rates of charge separation for PSII of different antenna size (Holzwarth *et al.* 1985, Schatz *et al.* 1987).

The primary charge separation reaction is one of the major pathways for dissipating excitation energy from excited singlet-state PSII reaction center: $P_{680}{}^{*}$.

$$v_1 = q[P_{680}{}^{*}\text{Pheo}]k^{o}_1 + [P_{680}{}^{*}\text{Pheo}](1-q)(1-p)k^{c}_1 + [P_{680}{}^{*}\text{Pheo}](1-q)pk^{o}_1 \qquad \ldots\ldots \quad (9)$$

$$\text{where } [P_{680}{}^{*}\text{Pheo}] = [U][P_{680}\text{Pheo}]\left(1+\frac{k_{-t}}{k_t}\right)^{-1}/70 \qquad \ldots\ldots \quad (10)$$

where q is the proportion of open reaction centers in all PSII reaction centers; $[P_{680}{}^{*}\text{Pheo}]$ is the concentration of excited singlet-state PSII reaction centers; *p* is the probability of migration of excitation energy from the core antenna of a closed reaction center to that of an open reaction center, k^{o}_1 is the rate constant of the primary charge separation reaction for open reaction centers; k^{c}_1 is the rate constant of the primary charge separation reaction for closed reaction centers. The rate constants of charge separation in closed (k^{c}_1) and open reaction center (k^{o}_1) are different. The k^{o}_1 is assumed to be $6.2k^{c}_1$, similarly, the rate constant for charge recombination increases by two fold upon the reduction of Q_A (Schatz et al., 1987). These changes in rate constants when Q_A is reduced have been suggested to be the result of a) altered electrical field by the negative charge on Q_A^{-} and b) the shorter distance between Q_A^{-} and Pheo than from Q_A^{-} to P_{680} (Dau, 1994).

This model assumes that PSII reaction centers are embedded in interconnected photosynthetic units, i.e. they are not isolated from each other (Deprez et al., 1990, Joliot & Joliot, 1964). A simple probability parameter (P) ranging from 0 to 1 is used in our

model to represent different probabilities of migration of excitation energy from core antennas of closed reaction centers to core antennas of open reaction centers.

4. The charge recombination reaction

The rate equation for the charge recombination reaction which involves the transfer of electron from $Pheo^-$ to P_{680}^+ is:

$$v_{-1} = q[P_{680}^+Pheo^-]k^o_{-1} + (1-q)[P_{680}^+Pheo^-]k^c_{-1} \quad \ldots\ldots \quad (11)$$

where v_{-1} is the charge recombination rate, and k^o_{-1} and k^c_{-1} represent rate constants for the charge recombination reaction between P_{680}^+ and $Pheo^-$ in open and closed PSII reaction centers respectively.

5. Excitation energy quenching by P_{680}^+

P_{680}^+ is a quencher of chlorophyll fluorescence (Butler, 1972). On a nanosecond to sub-nanosecond scale, the rise of Chl *a* fluorescence after a brief (< ns) actinic flash measures the electron flow from tyrosine to P_{680}^+ (Sonneveld et al., 1979). After illumination with a sequence of short light pulses, oscillation of fluorescence emission with a period of four was observed (Delosme, 1971). This phenomena is currently explained by the hypothesis that the oscillation of electrical fields, which stems from uncompensated positive charges of the OEC, influences the rate of electron transport from the tyrosine residue (Y_z) to P_{680}^+ and correspondingly P_{680}^+ quenching of chlorophyll fluorescence (Dau, 1994). In the current model, a rate constant (k_c) of 1 ns^{-1} was used to describe the quenching of Chl *a* fluorescence by P_{680}^+ (Trissl et al., 1993). The quenching of excitation energy in the core antenna is calculated as:

$$v_{P680qU} = [U]([P_{680}^+Pheo] + [P_{680}^+Pheo^-])k_c \quad \ldots\ldots \quad (12)$$

where [U] represents the concentration of excited singlet-state chlorophylls in PSII core antenna.

The quenching of excitation energy in the peripheral antenna is calculated as:

$$v_{P680qA} = [A]([P_{680}^+Pheo] + [P_{680}^+Pheo^-])k_c \quad \ldots\ldots \quad (13)$$

where [A] represents the concentration of excited singlet-state chlorophlls in PSII peripheral antenna (Trissl et al., 1993).

6. Excitation energy quenching by oxidized plastoquinone

Oxidized plastiquinone is also a strong quencher of chlorophyll fluorescence. Vernotte *et al.* (1979) found that if all the plastoquinone (PQ) pool is reduced, chlorophyll fluorescence emission is about 10~20% higher than when the PQ pool was oxidized (e.g. with addition of DCMU) under high light. In the current model, the rate constant for plastoquinone quenching is obtained based on the equation for the quantum yield of fluorescence,

$$\Phi_f = \frac{k_f}{k_f + k_d + k_q[PQ] + k_p[P_{680}Q_A]} \quad \ldots\ldots \quad (14)$$

where k_f, k_d, k_q, and k_p represent the rate constants for exciation energy deactivation in the form of fluorescence, heat dissipation, PQ quenching, and quenching by $P_{680}Q_A$ respectively (Reviewed: Govindjee, 1995). DCMU blocks electron transfer from Q_A to Q_B; therefore PQ under high light in the presence of DCMU is in the oxidized state. Assuming Q_A and PQ under high light without DCMU were all in the reduced state, the difference in fluorescence emission under high light with and without DCMU can be used to derive the empirical rate constant of plastoquinone quenching as following.
In the presence of DCMU, oxidation state of [PQ] is maximal since no electrons are transferred to PQ while k_p is zero, which leads to:

$$\Phi_{f1} = k_f/(k_f + k_d + k_q[PQT]) \quad \ldots\ldots \quad (15)$$

where $[PQT]_t$ represents the concentration of the PQ pool assuming all plastoquinone is reduced under strong light. Without DCMU, [PQ] and $[Q_A]$ are zero, which leads to:

$$\Phi_{f2} = k_f/(k_f + k_d) \quad \ldots\ldots \quad (16)$$

Considering that fluorescence emission is about 15% higher in the presence of DCMU than without (Vernotte et al., 1979), empirically then:

$k_q = 0.15(k_f + k_d)/ [PQT]$ …… (17)

The rate equation for quenching of excitation energy in the core antenna by oxidized plastoquinone is calculated as:

$v_{PQqU} = [U][PQ]k_q$ …… (18)

The rate equation for calculating the quenching of excitation energy in peripheral antenna by oxidized plastoquinone is calculated as:

$v_{PQqA} = [A][PQ]k_q$ …… (19)

7. Reactions of the oxygen evolving complex

The oxidized PSII reaction center, P_{680}^+ is reduced by Y_z of D1 protein. In this model, it is assumed that electrons pass through Y_z instantaneously. Therefore, electrons from different S states of oxygen evolution complex directly to P_{680}^+Pheo or $P_{680}^+Pheo^-$. For example, the rate of electron transfer from S_1 state of OEC to $P_{680}^+Pheo^-$ was calculated as:

$v_{1z\_1} = [S_{1T}]k_z[P_{680}^+Pheo^-]/[P_{680}PheoT]$ …… (20)

where k_z is the rate constant of electron transfer from Y_z to P_{680}^+, which is used here as the rate constant for electron transfer from OEC to P_{680}^+; $[S_{1T}]$ is the concentration of OEC in S_1 state before donating electron to P_{680}^+. $[P_{680}PheoT]$ represents the total concentration of different states of $P_{680}Pheo$ in PSII. The conversion between different consecutive S states of the OEC assumes first-order kinetics.

8. Reduction of Q_A

Reduced pheophytin reduces the electron acceptor Q_A. A first-order rate equation is used to describe this process. For example, electron transfer from $Pheo^+Pheo^-$ to Q_A was calculated as:

$v_{2\_1} = [P_{680}^+Pheo^-]k_2q$ …… (21)

where k_2 is the rate constant for this reaction. Our model incorporates the reverse electron transfer reaction from Q_A^- to Pheo using a pseudo-first-order rate equation. For example, the electron transfer rate from $Q_A^-Q_B$ to Pheo associated with P_{680}^+ was calculated as:

$v_{r2\_01\_1} = [Q_A^-Q_B]k_2 /Ke[P_{680}^+Pheo]/[P_{680}PheoT]$ ……(22)

where K_{e2} is the equilibrium constant for the electron transfer between Q_A and Pheo.

9. Exchange of plastoquinone

The exchange of plastoquinone between the Q_B site and the thylakoid membrane was calculated based on both the concentration of Q_B^{2-} and the redox state of plastoquinone pool in the thylakoid membrane, i.e.

$v_3 = [Q_AQ_B^{2-}]k_3[PQ]/[PQT]$ ……(23)

Where k_3 is the rate constant of the exchange.

10. Fluorescence emission

The total fluorescence emission from both the peripheral antenna and the core antenna complex is calculated as:

$\Phi_f = k^a_f A_p + ([U]+[U_i])k^u_f + k^a_f[A_{ip}] + k^a_u[U_{ifc}]$ …… (24)

Where k^a_f and k^u_f are the rate constants for fluorescence emission at the peripheral and core antenna respectively and Φ_f is the total fluorescence emission. $[U_i]$ is the concentration of excited singlet-state chlorophylls (including P_{680}^*) in the core antenna associated with inactive PSII center. $[A_{ip}]$ is the concentration of excitation energy on peripheral antenna of inactive photosystem II. $[U_{ifc}]$ is the concentration of excitation energy on chlorophylls detached from core antenna of inactive photosystem II.

NUMERICAL SIMULATION PROCEDURE

The rate of change of the concentration of each discrete reduction state of each intermediate or component in photosystem is represented by a differential equation. A differential equation for a component is derived by subtracting the sum of all rates consuming this component from the sum of all rates generating the component. All the

differential equations, describing rates of concentration change of all intermediates in photosystem, form a system of linked differential equations. This system of differential equations for the model is listed in Appendix I. The rate equations used in deriving the system of differential equations are described in the preceding section (*RATE EQUATIONS DESCRIBING EACH EXCITATION/ELECTRON TRANSFER REACTION*) and listed in Appendix II. This system of differential equations was solved using the *ode15s* procedure of MATLAB (the Mathworks, Inc. version 6, Natick, MA). This algorithm proved the most computationally efficient in dealing with this set of stiff differential equations. This algorithm is a variable order solver implementing implicit multistep method (Shampine & Reichelt, 1997). Estimates of the kinetic parameters were obtained from literature and from estimates as listed in Table 1. The concentrations of intermediates in the light reactions in dark-adapted C_3 leaves were used to initialize the model. It was assumed that all Q_A, Q_B, and plastoquinone are in an oxidized state for dark-adapted leaves.

In this study, we first compared the simulated fluorescence induction curve to a typical measured fluorescence induction curve, assuming all reaction centers are active. Then the origins of different phases of fluorescence induction curve were explored by comparing the fluorescence emission to the concentrations of different intermediates or compounds of photosystem. Thirdly the effects of modifying kinetic and structural parameters of PSII units on fluorescence induction kinetics were studied. Finally, the influences of different proportions of inactive PSII centers on fluorescence induction curve were explored.

RESULTS

Comparison of in silico and in vivo FI

The multi-phasic Chl *a* fluorescence induction curve predicted from the model when a leaf is excited with 3000 μmol photons m^{-2} s^{-1} mimics the experimentally recorded multiphasic O J I P transients (Fig. 2). The predicted fluorescence emission and the reduction status of Q_A do not change at the same rate (Fig. 3). Under a PPFD of 3000 μmol m^{-2} s^{-1}, Q_A approaches complete reduction much earlier than the predicted peak

value of fluorescence emission (Fig. 3) and the predicted fluorescence emission and the reduction status of Q_A do not change at the same rate.

OJIP in relation to the kinetics of redox of intermediates

The different phases of FI coincide with peak concentrations of oxidized or reduced forms of different components in the electron transfer chain. J coincides with the peak concentrations of $Q_A^-Q_B$ and $Q_A^-Q_B^-$; I with the first shoulder of $Q_A^-Q_B^{2-}$ concentration, and P with the peak concentrations of both $Q_A^-Q_B^{2-}$ and PQH_2 (Fig. 4).

The simulations showed that several factors influence the magnitude and shape of FI kinetics. Increasing the probability of excitation transfer from the core antenna of closed reaction centers to the core antenna of open reaction centers gradually delays the fluorescence increase from O to J without changing fluorescence emission at O (Fig. 5 b). Increasing the size of the peripheral antenna relative to the core antenna leads to higher fluorescence emission, and heat dissipation at O (Fig. 5 b). By increasing the initial concentration of S_0, the simulated J becomes more sharply defined. With oxygen evolving complex initially completely being in S_0 state, FI shows a dip after J (Fig. 5 c). The dip after J is eliminated if P_{680}^+ quenching of fluorescence is ignored (Fig. 6 a and 6 b). The fluorescence emission at J gradually increases and finally reaches I when the initial state of Q_B:Q_B^- is lowered from 1:0 to 0:1 (Fig. 6 d). Increasing the rate constant of plastoquinone oxidation (k_{ox}) and the PQ pool size in the thylakoid membrane decreases the fluorescence emission at P (Fig. 5 e and 5f).

The effects of inactive PSII centers on FI

Increasing the proportion of inactive reaction centers increased the fluorescence emission at O phase (Fig. 7a), as a result, F_v/F_m gradually decreases with increase in the proportion of inactive PSII (Fig. 7b).

DISCUSSION

Accepting the assumptions used in our model, when all discrete reactions of electron transfer from water-splitting through to cyt b_6f reduction are included, a realistic FI is simulated and several properties apparently determining the OJIP transients emerge. This model provides a new basis for extracting more information from the easily measured fluorescence induction transient (Table 3). Simulations based on this model showed that J corresponded to the peak concentrations of $Q_A^-Q_B$ and $Q_A^-Q_B^-$ and I to the first shoulder in the increase in concentration of $Q_A^-Q_B^{2-}$. The P peak coincided with maximum concentrations of both $Q_A^-Q_B^{2-}$ and PQH_2. In addition, simulations using this model suggest that different ratios of the peripheral antenna and core antenna lead to differences in fluorescence emission at O without affecting fluorescence emission at J I and P. Furthermore, increase inactive PSII center increase fluorescence emission at O phase and correspondingly decrease F_v/F_m.

Based on concentrations of intermediates of dark adapted leaves and rate constants for redox reactions and exciton transfer taken from the literature, this model predicts the multi-phasic Chl *a* FI curve (Fig. 2 a), including the distinct O J I P transients, closely mimicking observed FI kinetics (Fig. 2b). The current model is distinguished from previous models by incorporating each discrete step of energy and electron transfer around PSII. In addition, it differs from some previous models in that it uses the excited singlet-state chlorophyll molecules to predict fluorescence emission (Fig. 1). Furthermore, inclusion of the structural information for the core and the peripheral antenna enables the model to a) use PPFD directly as an input rather than using the rate of Q_A reduction (Stirbet et al., 1998), or the rate of excitation state formation (Lazar, 2003, Lebedeva et al., 2002); and b) examines the effect of different antenna structures on FI, which was not possible in the previous models (Table 2). Our model assumed that all the reaction centers are open on illumination, and predicts that fluorescence emission at O occurs before any reduction of Q_A (Fig. 3). This shows that FI occurs at different pace from Q_A reduction. The appearance of J was found to coincide most closely with the maximum concentrations of $Q_A^-Q_B$ and $Q_A^-Q_B^-$ (Fig. 4). This result is consistent with the

experimental and theoretical results showing that the O-J phase is largely driven by primary photochemistry, i.e. reduction of the primary electron acceptor in PSII, pheophytin, and the first quinone electron acceptor of PSII, Q_A (Delosme, 1967, Lazar et al., 1998, Lazar et al., 1997, Neubauer & Schreiber, 1987, Stirbet et al., 1998, Strasser et al., 1995). Consistent with the model of Stirbet et al. (1998), the inflexion point I was found to correspond to the first inflexion in the concentration of $Q_A^-Q_B^{2-}$ (Fig 4 c). The concentration of $Q_A^-Q_B^{2-}$ was maximal at P (Fig. 4 c). At the same time, the plastoquinone pool was also maximally reduced at point P (Fig. 4 d). Models of FI lacking a description of the electron transfer reactions beyond Q_A reduction, i.e. the Q_B reduction and plastoquinone reduction reactions, cannot simulate the I-P phase (Schreiber & Krieger, 1996, Trissl & Lavergne, 1995, Vredenberg, 2000). Therefore, the appearance of the I-P phase possibly requires the accumulation of double-reduced Q_B and the reduced plastoquinone pool molecules.

In our model the connectivity between closed and open reaction centers is described using a simple empirical probability parameter *p* (Eqn. 9). With a higher *p* value, the connectivity between open and closed reaction centers is higher. As in the model of Stirbet *et* al (1998), increasing *p* gradually delays the fluorescence increase from O to J without changing emission at O. This suggests that increased connectivity between core antennas of closed and open reaction centers will decrease the loss of excitation energy as fluorescence and heat, and leads to a higher efficiency of excitation energy utilization. In contrast to the O-J phase, the fluorescence intensities in the I-P phase are not detectably influenced by *p* within the current model, which differs from the predictions of the model of Stirbet *et al.* (1998).

Simulations with the current model suggest that the "structure" of the light harvesting complex influences F_o without apparent changes in the fluorescence emissions at points J, I and P. A relatively greater peripheral antenna compared to core antenna leads to higher F_o (Fig. 5 b). This result provides another mechanism to alter the commonly used fluorescence parameter, F_v/F_m, where $F_v = F_m - F_o$ and F_m is the maximum fluorescence emission under saturating light. Based on this result, F_v/F_m can be altered through

changes in the relative size of core antenna and peripheral antenna without any change in the rate constant of charge separation in the PSII reaction center. Specifically, a relatively smaller size of peripheral antenna compared to core antenna might be preferred for higher efficiency of excitation energy utilization (Fig. 5b). In this respect, it is surprising to note that the amount of chlorophyll in the peripheral antenna is nearly three times or more than that in the core antenna (Horton et al., 1996, Peter & Thornber, 1991). This point to a possibility to genetic manipulations of antenna structures to potentially increase excitation energy utilization and correspondingly the photosynthetic carbon fixation for leaves of shade environments, e.g. leaves of understory plants or leaves in the lower layers of canopy.

With increase in the initial concentration of S_0, the point J becomes more distinct. A dip after point J correspondes most strongly to a high initial concentration of S_0 (Fig. 5 c). Similar results have been reported by Stirbet *et al* (1998). Considering the differences in the rate of transitions between different states of OEC, especially the slower transition between S_0 and S_1, Lazar (Lazar, 2003) has suggested that the dip after I reflects a momentary accumulation of P_{680}^+, which is a strong quencher of fluorescence. This is confirmed in our simulations where ignoring P_{680}^+ quenching of fluorescence eliminates the dip after point J in FI when initial concentration of S_0 is high (Fig. 6 a). On the contrary, when the initial concentration of S_1 is high, the transition between S_1 and S_2 is fast enough to provide electrons to P_{680}^+ and therefore prevent accumulation of P_{680}^+ and correspondingly quenching of fluorescence by P_{680}^+ (Fig. 6 b). The S_1:S_0 ratio for dark-adapted leaves has been suggested to range from 3:1 to 1:0 (Haumann & Junge, 1994, Kok et al., 1970, Messinger & Ranger, 1993), which should not lead to a dip after J if the transition between S_1 and S_2 is fast enough. Therefore, a recorded dip in FI for dark adapted leaves might indicate a decrease in the rate constant of the transition between S_1 and S_2 states in an oxygen evolution complex, or a decrease in the ratio of S_1:S_0, which causes transient accumulation of P_{680}^+.

Changing Q_B:Q_B^- ratio influences the appearance of point J in FI. As shown in Fig. 4b, the fluorescence emission at the point J gradually increases and finally reaches the

fluorescence emission of point I when the initial state of Q_B:Q_B^- is changed from 1:0 to 0:1 (Fig. 6 d). Therefore, the relative redox state of Q_B appears to determine the fluorescence emission at point J relative to point I in FI. A Q_B:Q_B^- of 0.5:0.5 is consistent with that reported for dark-adapted leaves (Rutherford et al., 1984).

The fluorescence emission at point P is influenced by both the rate constant of plastoquinone oxidation (k_{ox}) (Fig. 5 e) and the pool size of plastoquinone (Fig. 5 f). The fluorescence emission at point P reflects a balance between the rate of incident excitation energy at the PSII side and the rate of utilization of the chemical (potential) energy and the rate of heat dissipation. In our model, PQH_2 oxidation by the cytochrome b_6f complex (with a rate constant k_{ox}) represents the final fate of the chemical energy. Higher k_{ox} leads to a higher rate of energy utilization, which indirectly decreases the amount of excitation energy available for dissipation as fluorescence since more energy can be utilized in photochemistry. Furthermore, higher k_{ox} increases the oxidation state of PQ at steady state under a given light flux. Higher oxidized PQ concentration quenches excitation energy and therefore lowers fluorescence emission (Govindjee, 1995, Vernotte et al., 1979) (Fig. 5 e). Therefore, changes in the fluorescence emission at P for a leaf sample under certain treatment can be used to monitor the changes in PQH_2 oxidation. Changes in the PQ pool size change fluorescence emission at P level (Fig. 5f). Increases in the PQ pool size in the thylakoid membrane leads to higher oxidized PQ concentration, which results in decreased fluorescence emission at P (Fig. 5 f).

Finally, changes in the proportion of inactive PSII centers lead to changes in F_v/F_m (Fig. 7). There are many experimental evidences showing decreased F_v/F_m upon increase in proportion of inactive PSII centers (Critchley & Russell, 1994, Hong & Xu, 1999, Melis, 1985). In this model, with increase in the proportion of inactive PSII centers, more excitation energy is incident is absorbed by the core antennae of inactive PSII centers and chlorophylls in peripheral antennas detached from the inactive center. Therefore, a higher proportion of the incident energy is diverted into fluorescence and heat dissipation rather than being utilized in primary charge separation. As a result, increase in the proportion of

inactive PSII centers increases fluorescence emission at the O phase (Fig. 7), which lead to decrease in F_v/F_m.

Acknowledgement: This work is co-supported by the National Center for Supercomputing Applications, and the U. S. National Science Foundation IBN 04-17126. We thank Dr. Morgan P.B., Ainsworth E.A., Bernacchi C.J., Heaton E.A., Dr. Shawna N. , Castro J., and Chen C. for useful comments on the manuscript.

LITERATURE

Baake E & Schloder JP (1992) Modeling the fast fluorescence rise of photosynthesis. Bulletin of Mathematical Biology, **54**, 999-1021.

Baker NR, East TM & Long SP (1983) Chilling damage to photosynthesis in young *Zea mays*. Journal of Experimental Botany, **34**, 189-197.

Bolhár-Nordenkampf HR, Long SP, Baker NR, Qquist G, Schreiber U & Lechner EG (1989) Chlorophyll fluorescence as a probe of the photosynthetic competence of leaves in the field - a review of current instrumentation. Functional Ecology, **3**, 497-514.

Bowes J & Crofts AR (1980) Binary oscillations in the rate of reoxidation of the primary acceptor of photosystem II. Biochimica et Biophysica Acta, **590**.

Brody SS (2002) Fluorescence lifetime, yield, energy transfer and spectrum in photosynthesis, 1950-1960. Photosynthesis research, **73**, 127-132.

Butler WL (1972) On the primary nature of fluorescence yield changes associated with photosynthesis. Proceedings of the National Academy of Sciences of the United States of America, **69**, 3420-3422.

Chitnis PR (2001) Photosystem I: function and physiology. Annual of Plant Physiology and Plant Molecular Biology, **52**, 593-636.

Chylla RA & Whitmarsh J (1990) Light saturation response of inactive photosystem-II reaction centers in spinach. Photosynthesis Research, **25**, 39-48.

Critchley C & Russell AW (1994) Photoinhibition of Photosynthesis in-Vivo - the Role of Protein-Turnover in Photosystem-Ii. Physiologia Plantarum, **92**, 188-196.

Crofts AR, Robinson HH & Snozzi M (1984) Reactions of quinones at catalytic sites: a diffusional role in H-transfer. In Sybesma C (ed) Advances in Photosynthesis Research. volume 1. Martinus Nijhoff/Dr W. Junk Publishers, The Hague, Netherlands. pp461-468.

Dau H (1994) Molecular mechanisms and quantitative models of variable photosystem II fluorescence. Photochemistry and Photobiology, **60**, 1-23.

Dekker JP, Plijter JJ, Ouwehand L & van Gorkom HJ (1984) Kinetics of maganses redox transitions in the oxygen evolving complex of photosystem II. Biochemica et Biophysica Atca, **767**, 176-179.

Delosme R (1967) Etude de l'induction de fluorescence des algues vertes et des chloroplasts au debut d'une illumination intense. Biochimica et Biophysica Acta, **143**, 108-128.

Delosme R (1971) New results about chlorophyll fluorescence *in vivo.* In Forti G, Avron M and Melandri A (eds) Proceedings of the 11th International Congress on Photosynthesis Research. volume 1. Martinus Nijhoff/Dr W. Junk, The Hague, Netherlands. pp187-95.

Deprez J, Paillotin G, Dobek A, Leibl W, Trissl HW & Breton J (1990) Competition between energy trapping and exciton annihilation in the lake model of the photosynthetic membrane of purple bacteria. Biochimica et Biophysica Acta, **1015**, 295-303.

Forbush B, Kok B & McGloin MP (1971) Cooperation of charges in photosynthetic O_2 evolution. II. Damping of flash yield oscillation and deactivation. Photochemistry and Photobiology, **14**, 307-321.

Golbeck JH & Kok B (1979) Redox titration of electron acceptor Q and the plastoquinone pool in photosystem II. Biochimica et Biophysica Acta, **547**, 347-360.

Govindjee (1995) Sixty -three years since Kautsky: Chlorophyll a fluorescence. Australian Journal of Plant Physiology, **22**, 131-160.

Hankamer B, Barber J & Boekema EJ (1997) Structure and membrane organization of photosystem II in green plants. Annual Review of Plant Physiology and Plant Molecular Biology, **48**, 641-671.

Haumann M & Junge W (1994) Extent and rate of proton release by photosynthetic water oxidation in thylakoids: electrostatic relaxation versus chemical production. Biochemistry, **33**, 864-872.

Hong SS & Xu DQ (1999) Light-induced increase in initial chlorophyll fluorescence Fo level and the reversible inactivation of PSII reaction centers in soybean leaves. Photosynthesis Research, **61**, 269-280.

Horton P, Ruban AV & Walters RG (1996) Regulation of light harvesting in green plants. Annual Review of Plant Physiology and Plant Molecular Biology, **47**, 655-684.

Joliot A & Joliot P (1964) Etude cinetique de la reaction photochimique liberant l'oxygene au cous de la photosynthese. Computes Rendue Academie Science Paris, **258**, 4622-4625.

Kok B, Forbush B & McGloin MP (1970) Cooperation of charges in photosynthetic O_2 evolution. I. A linear four step mechanism. Photochemistry and Photobiology, **11**, 457-475.

Kramer DM, Dimarco G & Loreto F (1995) Contribution of plastoquinone quenching to saturation pulse-induced rise of chlorophyll fluorescence in leaves. In Mathis P (ed). Photosynthesis from light to the biospere. volume 1. Kluwer Academic Publishers, Dordrecht. pp147-150.

Krause GH & Weis E (1991) Chlorophyll fluorescence and photosynthesis - the basics. Annual Review of Plant Physiology and Plant Molecular Biology, **42**, 313-349.

Lavergne J & Trissl HW (1995) Theory of fluorescence induction in photosystem II - Derivation of analytical expressions in a model including exciton-radical- pair equilibrium and restricted energy transfer between photosynthetic units. Biophysical Journal, **68**, 2474-2492.

Lazar D (1999) Chlorophyll a fluorescence induction. Biochimica et Biophysica Acta-Bioenergetics, **1412**, 1-28.

Lazar D (2003) Chlorophyll a fluorescence rise induced by high light illumination of dark-adapted plant tissue studied by means of a model of photosystem II and considering photosystem II heterogeneity. Journal of Theoretical Biology, **220**, 469-503.

Lazar D, Brokes M, Naus J & Dvorak L (1998) Mathematical modelling of 3-(3', 4'-dichlorophenyl)-1,1-dimethylurea action in plant leaves. Journal of Theoretical Biology, **191**, 79-86.

Lazar D, Naus J, Matouskova M & Flasarova M (1997) Mathematical modeling of changes in chlorophyll fluorescence induction caused by herbicides. Pesticide Biochemitry and Physiology, **57**, 200-210.

Lazar D & Pospisil P (1999) Mathematical simulation of chlorophyll a fluorescence rise measured with 3-(3 ',4 '-dichlorophenyl)-1,1-dimethylure barley leaves at room and high temperatures. European Biophysics Journal, **28**, 468-477.

Lebedeva GV, Belyaeva NE, Demin OV, Riznichenko GY & Rubin AB (2002) Kinetic model of primary photosynthetic processes in chloroplasts. Description of the fast phase of chlorophyll fluorescence induction under different light intensities. Biophysics, **47**, 968-980.

Melis A (1985) Functional properties of photosystem II beta in spinach chloroplasts. Biochimica et Biophysica Acta, **808**, 334-342.

Messinger J & Ranger G (1993) Generation, oxidation by the oxidized form of the tyrosine of polypeptide D2, and possible electronic configuration of the redox states S_0, S_1 and S_2 of the water oxidase in isolated spinach thylakoids. Biochemistry, **32**, 9379-9386.

Neubauer C & Schreiber U (1987) The polyphasic rise of chlorophyll fluorescence upon onset of strong continous illumination: I. Saturation charactristics and partial control by photosystem II acceptor side. Zeitschrift für Naturforschung, **42c**, 1426-1254.

Peter GF & Thornber JP (1991) Biochemical composition and organization of higher plant photosystem II light harvesting pigment proteins. Journal of Biological Chemistry, **266**, 16745-16754.

Roelofs TA, Lee CH & Holzwarth AR (1992) Global target analysis of picosecond chlorophyll fluorescence kinetics from pea chloroplasts - a new approach to the characterization of the primary processes in photosystem II α units and β units. Biophysical Journal, **61**, 1147-1163.

Rohacek K & Bartak M (1999) Technique of the modulated chlorophyll fluorescence: basic concepts, useful parameters, and some applications. Photosynthetica, **37**, 339-363.

Rutherford W, Govindjee & Inoue Y (1984) Charge accumulation and photochemistry in leaves studied by thermoluminescence and delayed light emission. Proceedings of the National Academy of Sciences of the United States of America, **81**, 1107-1111.

Sayed OH (2003) Chlorophyll fluorescence as a tool in cereal crop research. Photosynthetica, **41**, 321-330.

Schatz GH, Brock H & Holzwarth AR (1987) Picosecond kinetics of fluorescence and absorbency changes in photosystem II particles excited at low photon density. Proceedings of the National Academy of Sciences of the United States of America, **84**, 8414-8418.

Schatz GH, Brock H & Holzwarth AR (1988) Kinetics and energetic model for the primary processes in photosystem II. Biophysical Journal, **54**, 397-405.

Schreiber U & Krieger A (1996) Two fundermentally different types of variable chlorophyll fluorescence *in vivo*. FEBS Letter, **397**, 131-135.

Shampine LF & Reichelt MW (1997) The MATLAB ODE suite. SIAM Journal on Scientific Computing, **18**, 1-22.

Sonneveld A, Rademaker H & Duysens LNM (1979) Chlorophyll *a* fluorescence as a monitor of nanosecond reduction of the photooxidized primary donor P_{680}^{+} of photosystem II. Biochimica et Biophysica Acta, **548**, 536-551.

Stirbet A, Govindjee, Strasser BJ & Strasser R (1998) Chlorophyll a fluorescence induction in higher plants: Modelling and numerical simulation. Journal of Theoretical Biology, **193**, 131-151.

Stirbet A & Strasser RJ (2001) The possible role of pheophytine in the fast fluorescence risk OKJIP. In: *Proceedings of the 12th International Congress on Photosynthesis* (CD-ROM), S11-027, CSIRO Publishing, Collingwood.

Strasser RJ, Srivastava A & Govindjee (1995) Polyphasic chlorophyll a fluorescence transient in plants and cyanobacteria. Photochemistry and Photobiology, **61**, 32-42.

Trissl HW, Gao Y & Wulf K (1993) Theoretical fluorescence induction curves derived from coupled differential equations describing the primary photochemistry of photosystem II by an exciton radical pair equilibrium. Biophysical Journal, **64**, 974-988.

Trissl HW & Lavergne J (1995) Fluorescence induction from photosystem II - analytical equations for the yields of photochemistry and fluorescence derived from analysis of a model including exciton-radical pair equilibrium and restricted energy-

transfer between photosynthetic units. Australian Journal of Plant Physiology, **22**, 183-193.

Vavilin DV, Tyystjarvi E & Aro EM (1998) Model for the fluorescence induction curve of photoinhibited thylakoids. Biophysical Journal, **75**, 503-512.

Velthuys BR & Amesz J (1974) Charge accumulation at the reducing side of system II of photosynthesis. Biochimica et Biophysica Acta, **325**, 138-148.

Vernotte C, Etienne AL & Briantais JM (1979) Quenching of the system II chlorophyll fluorescence by the plastoquinone pool. Biochimica et Biophysica Acta, **545**, 519-527.

Vredenberg WJ (2000) A three-state model for energy trapping and chlorophyll fluorescence in photosystem II incorporating radical pair recombination. Biophysical Journal, **79**, 26-38.

FIGURE LEGEND

Figure 1

Block flow diagram of the steps underlying chlorophyll fluorescence induction on a dark-light transition. In this diagram, only the reactions associated with one active PSII unit is included. Each illustrated step is represented by a differential equation in the model. Change in the concentration of each component illustrated is achieved by numerical integration of these linked equaitons. The section enclosed by the dotted line represents the charge separation process in the PSII reaction center. U^o and U^c represent the singlet-excited chlorophylls within the core antenna associated with the open and closed reaction center respectively. S_1, S_2, S_3, and S_4 represent the four redox states of the oxygen evolving complex (OEC). Y_z: primary electron donor for photosystem II reaction center (P_{680}). Phe: pheophytin. PQ: plastoquinone; PQH_2: plastoquinol; Q_A: the first quinone electron acceptor in PSII; Q_B: the second quinone electron acceptor in PSII; cyt b6f: cytochrome b_6f complex.

Figure 2

The fluorescence emission predicted by the current model (a) compared to the experimentally recorded fluorescence induction curve (b, Strasser *et al.* 1995). The x axis is the logarithm of time with time using second as unit. The input photon flux density (PFD) used for the simulation is 3000 μmol photons m^{-2} s^{-1} (sunlight). The kinetic parameters used in the simulation are listed in Table 5.1. The initial concentrations of different electron carrier in the dark were assumed to be: a) Q_A and Q_B are completely oxidized; b) photosystem II reaction centers are all in P_{680}Phe state; c) oxygen evolution complexes are in the state of either S1 or S2 with a ratio of 4:1; d) the ratio of PQ: PQH_2 in thylakoid membrane is 1:1. In the simulation, all PSII reaction centers are assumed to be active. The radiant flux used in the experiment was 600 W m^{-2} (Strasser *et al*., 1995), which corresponds to a photon flux density of 3255 μmol photons (λ=650 nm) m^{-2} s^{-1}.

Figure 3

The predicted fluorescence induction curve and the corresponding proportion of reduced Q_A. The x axis is the logarithm of time with time using second as unit. The proportion of reduced Q_A is calculated as: $[Q_A^-]/([Q_A]+ [Q_A^-])$; where where $[Q_A] = [Q_AQ_B]+[Q_AQ_B^-]+[Q_AQ_B^{2-}]$ and $[Q_A^-] = [Q_A^-Q_B] + [Q_A^-Q_B^-] + [Q_A^-Q_B^{2-}]$.
The input photon flux density and simulation conditions are as Fig. 2. a: predicted fluorescence induction curve; b: predicted proportion of Q_A reduction.

Figure 4

The predicted fluorescence emission and the corresponding changes in concentrations of different components involved in the primary events of PSII. The x axis is the logarithm of time and the unit for time is second. The input photon flux density and simulation conditions were as in Fig. 2. The components plotted in these four panels are sequentially, a: $Q_A^-Q_B$; b: $Q_A^-Q_B^-$; c: $Q_A^-Q_B^{2-}$; d) PQH_2. In panel D, the fluorescence emission assuming no PQ quenching, is also included as indicated as $F^u(t)$. The fluorescence emission with PQ quenching represented as F(t).

Figure 5

The predicted influences of different structural and kinetic parameters on the shape of the fluorescence induction curve. The input photon flux density and simulation conditions were as in Fig. 2. a) Probability of excitation transfer from core antenna of closed reaction centers to that of open reaction centers; b) the ratio of the number of chlorophylls in core antenna to that in peripheral antenna; c) the ratio of the initial concentration of S_1 state to S_0 state of the oxygen evolution complex; d) the ratio of initial concentration of Q_B to initial concentration of Q_B^-; e) the rate constant of PQH_2 oxidation; f) the pool size of plastoquinone (PQ) in thylakoid membrane.

Figure 6

The predicted fluorescence induction curve with and without quenching by P_{680}^+. The condition used for simulations were same as Fig. 2. The simulations were done for two

different initial $[S_1]:[S_0]$ of oxygen evolution complexes (a: $[S_1]:[S_0] = 0.1:0.9$; b: $[S_1]:[S_0] = 0.8:0.2$). There was no detectable difference between the shapes of fluorescence induction curves regardless of whether P_{680}^+ quenching is or is not included if the initial ratio of S_1 to S_0 is 0.8:0.2.

Figure 7

The effects of the percentage of inactive PSII reaction center ($x/(1+x)$ with x being the ratio of inactive to active PSII reaction center) on (a) fluorescence induction curve and (b) F_v/F_m, or $(F_m-F_o)/F_m$ where F_m and F_o are the fluorescence emission at P and O phase respectively obtained from Fig. 7a. The input photon flux density and simulation conditions used for simulations were same as Fig. 2. The maximum fluorescence emission is scaled to be the same level.

FIGURES AND TABLES

Figure 1

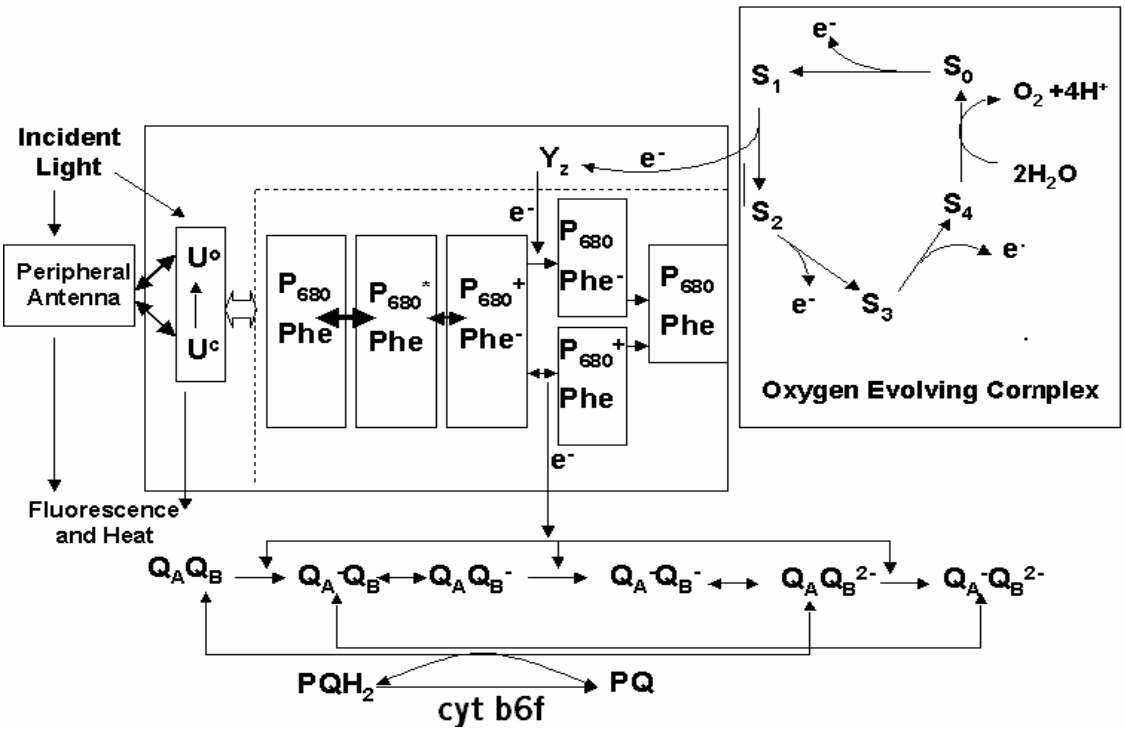

Figure 2

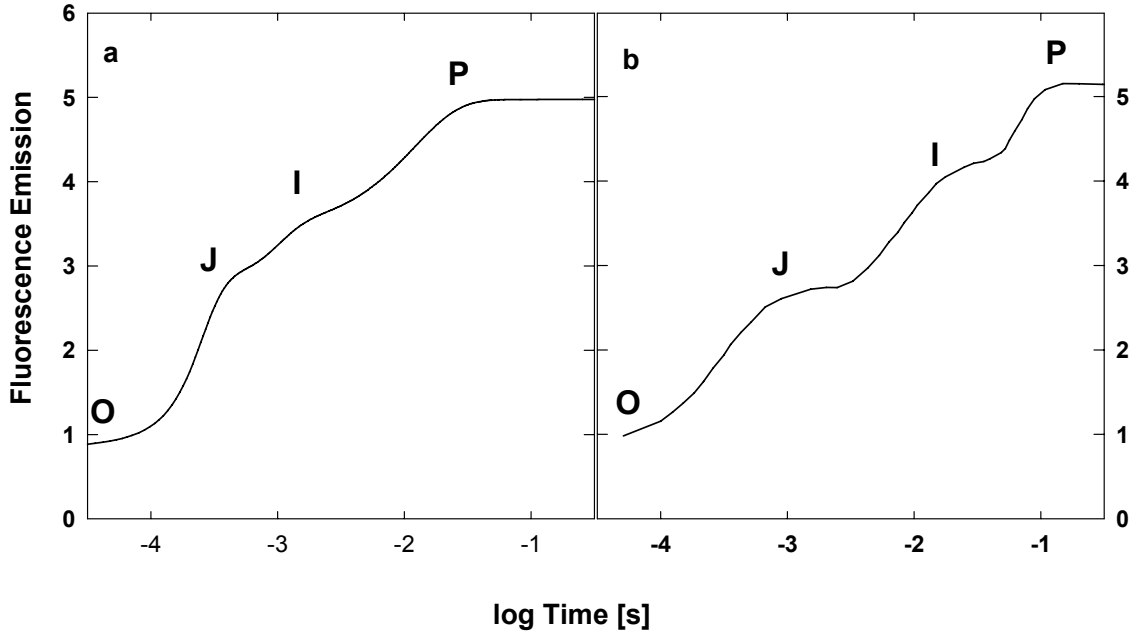

Figure 3

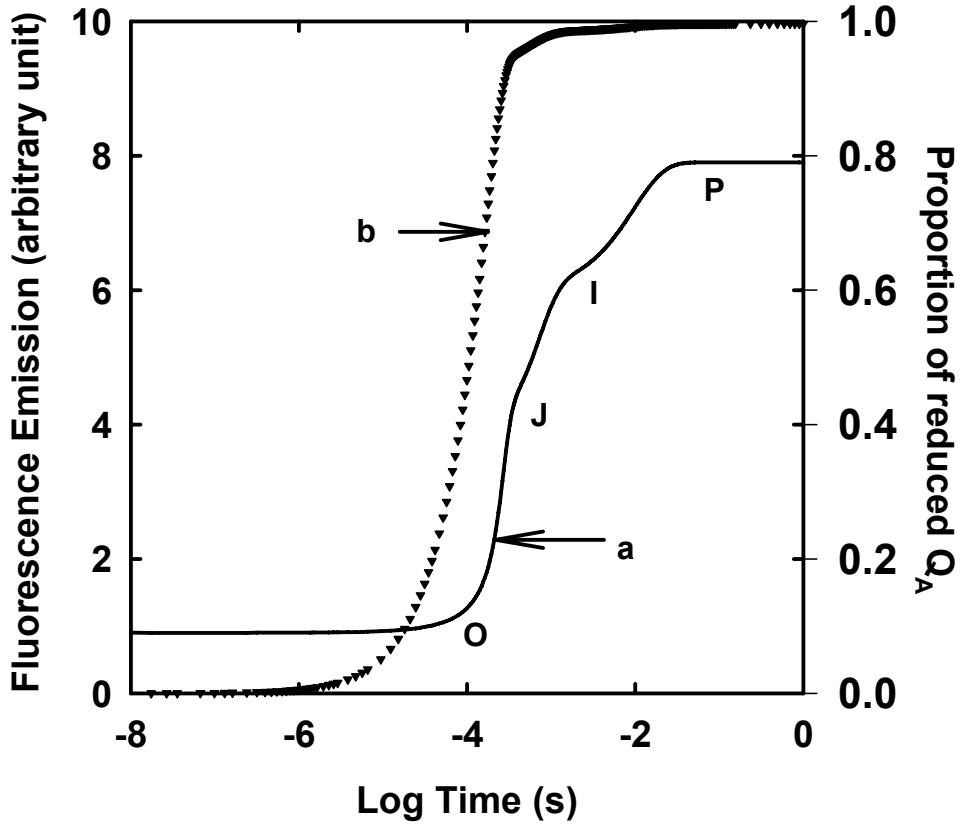
Fluorescence Emission (arbitrary unit)
Proportion of reduced Q_A
Log Time (s)
10
8
6
4
2
0
1.0
0.8
0.6
0.4
0.2
0.0
-8
-6
-4
-2
0
b
a
O
J
I
P

Figure 4

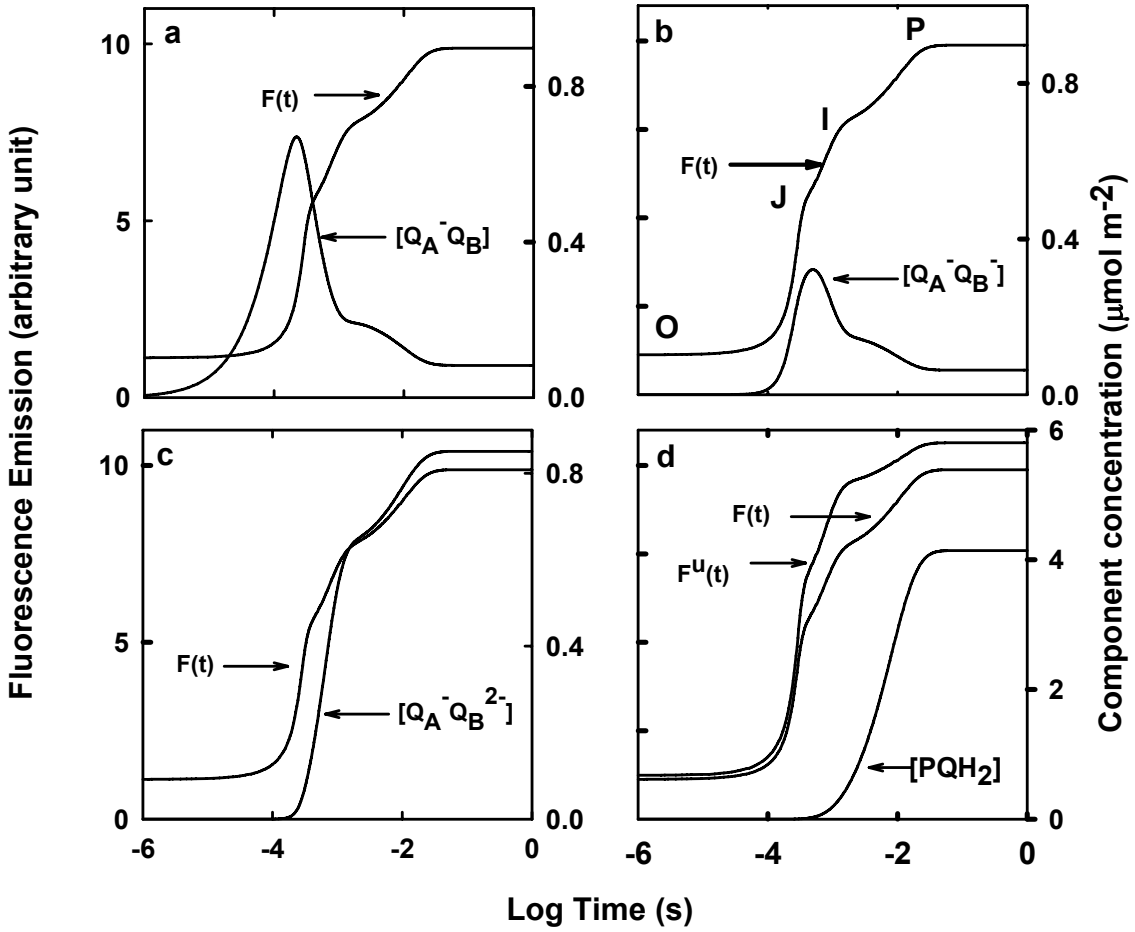
a
b
c
d
P
I
J
O
F(t)
$[Q_A^-Q_B]$
$[Q_A^-Q_B^-]$
$[Q_A^-Q_B^{2-}]$
$F^u(t)$
$[PQH_2]$
Fluorescence Emission (arbitrary unit)
Component concentration (µmol m^{-2})
Log Time (s)
10
5
0
0.8
0.4
0.0
6
4
2
-6
-4
-2
0

Figure 5

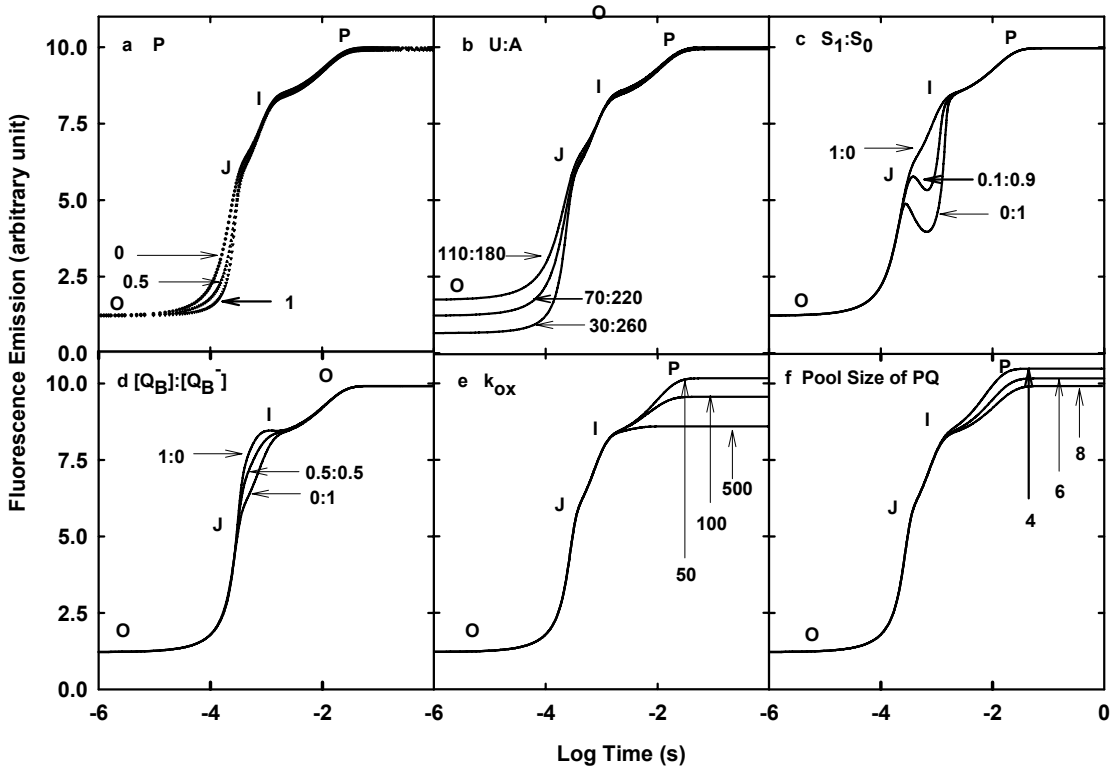
a P
b U:A
c S_1:S_0
d [Q_B]:[Q_B^-]
e k_{ox}
f Pool Size of PQ
O
J
I
P
0
0.5
1
110:180
70:220
30:260
1:0
0.1:0.9
0:1
0.5:0.5
50
100
500
4
6
8
Fluorescence Emission (arbitrary unit)
Log Time (s)
10.0
7.5
5.0
2.5
0.0
-6
-4
-2
0

Figure 6

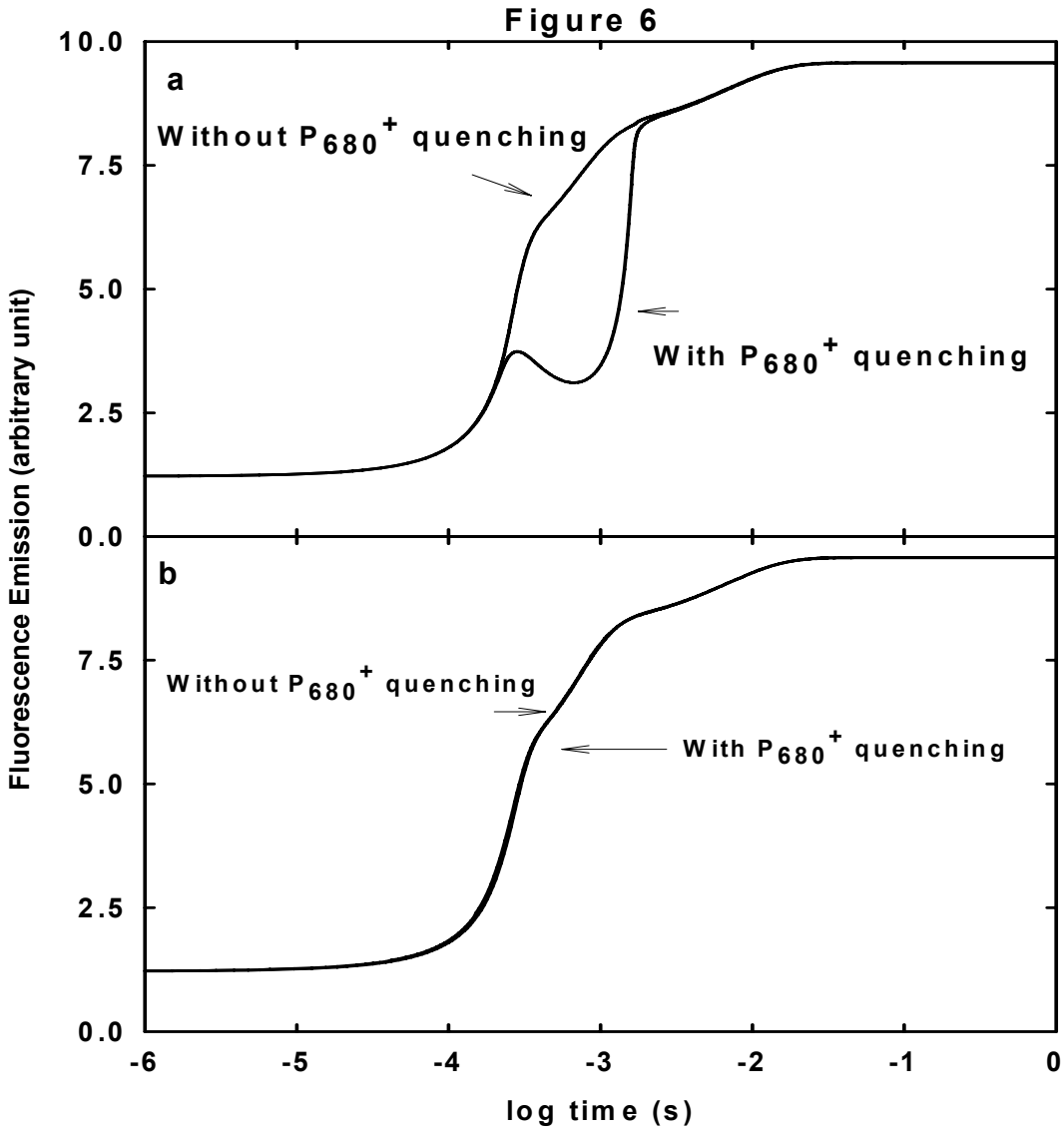
Figure 6
a
Without P_{680}^+ quenching
With P_{680}^+ quenching
b
Without P_{680}^+ quenching
With P_{680}^+ quenching
Fluorescence Emission (arbitrary unit)
log time (s)
10.0
7.5
5.0
2.5
0.0
-6
-5
-4
-3
-2
-1
0

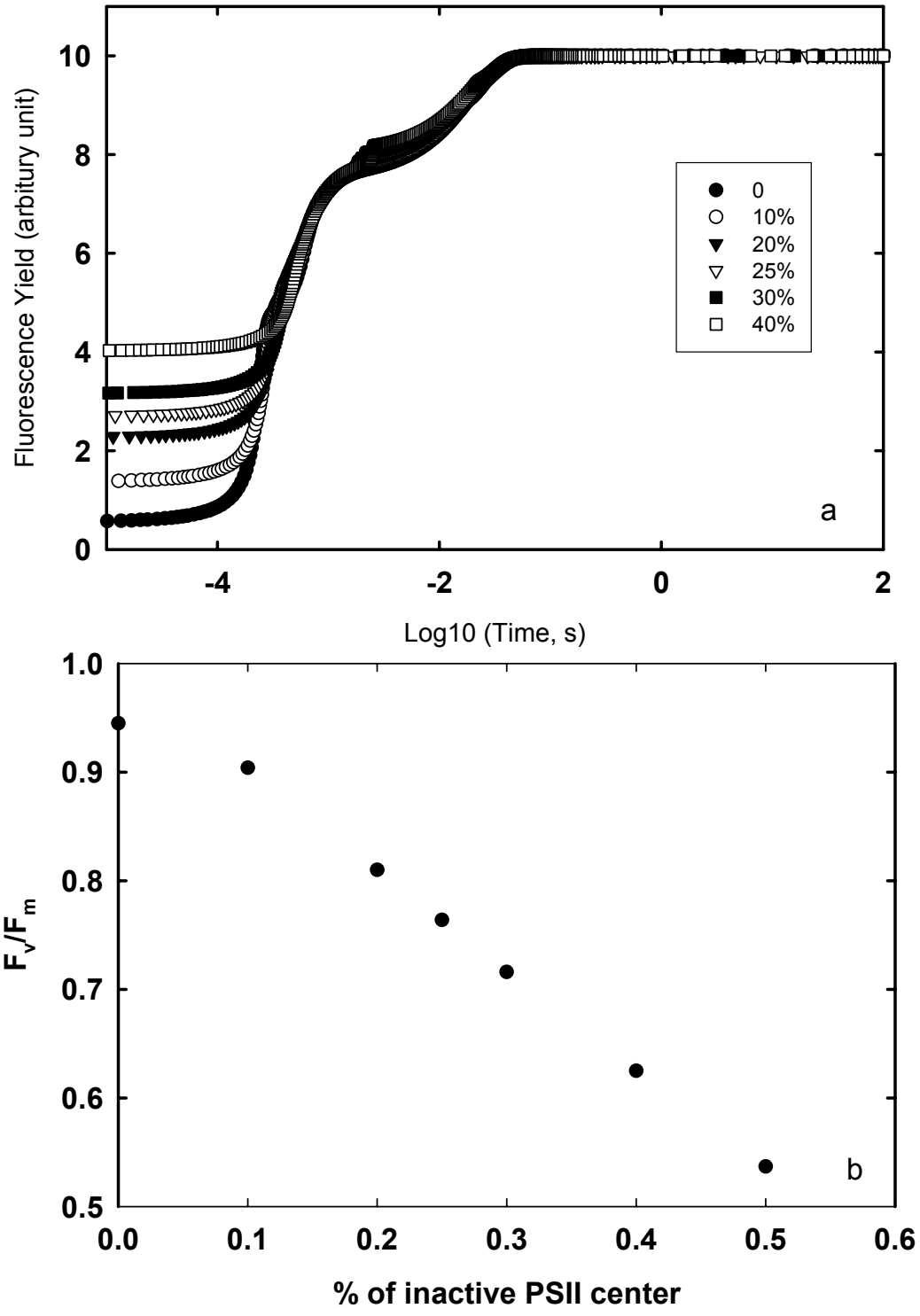
Fluorescence Yield (arbitury unit)
10
8
6
4
2
0
-4
-2
0
2
Log10 (Time, s)
0
10%
20%
25%
30%
40%
a
F_v/F_m
1.0
0.9
0.8
0.7
0.6
0.5
0.0
0.1
0.2
0.3
0.4
0.5
0.6
% of inactive PSII center
b

Figure 7

Table 1

Parameters used in the model of fluorescence induction.

Description	**Abbr.**	**Typical value**	**Reference**
Incident photon flux density	I_{in}	3,000 μmol m^{-2} s^{-1}	
The probability of the migration of excitation energy from core antenna of closed reaction centers to that of open reaction centers	p	0~1	Empirical parameter for our model
Speed of light	c	3×10^8 m s^{-1}	
Planck's constant	h	6.62×10^{-34} J s	
Boltzmann constant	k	1.38×10^{-23} J K^{-1}	
Rate constant of electron transfer from $Pheo^-$ to Q_A	k_2	2×10^9 s^{-1}	(Lazar & Pospisil, 1999, Roelofs et al., 1992)
Rate constant of the exchange of PQ with Q_B^{2-}	k_3	800 s^{-1}	(Lazar, 1999)
Rate constant of electron transfer from Q_A^- to Q_B	k_{AB1}	2500 s^{-1}	(Lazar, 1999)

Rate constant of electron transfer from Q_A^- to Q_B^-	k_{AB2}	$3300\ s^{-1}$	(Lazar, 1999)
Rate constant of heat dissipation in peripheral antenna system	k^a_d	$10^8\ s^{-1}$	(Lavergne & Trissl, 1995, Lazar, 1999) (Brody, 2002,
Rate constant for fluorescence emission from peripheral antenna	k^a_f	$3\times10^7\ s^{-1}$	Lavergne & Trissl, 1995)
Rate constant of excitation energy transfer from core antenna to peripheral antenna	k_{UA}	$10^{10}\ s^{-1}$ *	Model estimate
Rate constant of electron transfer from Q_B^- to Q_A	k_{BA1}	$175\ s^{-1}$	(Lazar, 1999)
Rate constant of electron transfer from Q_B^{2-} to Q_A	k_{BA2}	$250\ s^{-1}$	(Lazar, 1999)
Rate constant of excitation energy quenching by P_{680}^+	k_c	10^9 $s^{-1}\ (\mu mol\ m^{-2})^{-1}$	(Trissl et al., 1993)
Rate constant of charge recombination between $Pheo^-$ and P_{680}^+ in closed PSII reaction centers	k^c_{-1}	$9\times10^8\ s^{-1}$	(Roelofs et al., 1992)

Rate constant of charge separation of closed PSII reaction centers	k^c_1	4×10^9 s^{-1}	(Roelofs et al., 1992)
Equilibrium constant for electron transfer between Pheo and Q_A	Ke	10^6	Model estimate
Rate constant of transition from S_o to S_1 state	k_{o01}	50 s^{-1}	(Dekker et al., 1984)
Rate constant of charge recombination between $Pheo^-$ and P_{680}^+ in open PSII reaction center	k^o_{-1}	3×10^8 s^{-1}	(Roelofs et al., 1992)
Rate constant of transition from S_1 to S_2 state	k_{o12}	30,000 s^{-1}	(Dekker et al., 1984)
Rate constant of transition from S_2 to S_3 state	k_{o23}	10,000 s^{-1}	(Dekker et al., 1984)
Rate constant of transition from S_3 to S_0 state	k_{o30}	3000 s^{-1}	(Dekker et al., 1984)
Rate constant of charge separation in open PSII reaction center	k^o_1	2.5×10^{10} s^{-1}	(Roelofs et al., 1992)
Rate constant of PQH_2 oxidation	k_{ox}	50~500 s^{-1}	(Lazar, 1999)
Rate constant of excitation energy quenching by oxidized plastoquinone	k_q	3×10^6 s^{-1} $(\mu mol\ m^{-2})^{-1}$	Model estimate
	k_{r3}	80~800 s^{-1}	(Crofts et

Rate constant of the exchange of PQH_2 with Q_B			al., 1984, Golbeck & Kok, 1979)
Rate constant of excitation energy transfer from core antenna to reaction center of PSII	k_t	Implicit	s^{-1}
Rate constant of excitation energy transfer from reaction center to core antenna of PSII	k_{-t}	Implicit	s^{-1}
Rate constant of excitation energy transfer from peripheral antenna to core antenna of PSII	k_{AU}	10^{10} s^{-1} *	Model estimate
Rate constant of heat dissipation in core antenna associated with closed PSII reaction centers	k^{Uc}_d	10^8 s^{-1}	(Lazar & Pospisil, 1999, Roelofs et al., 1992)
Rate constant for fluorescence emission from core antenna of PSII	k^U_f	3×10^7 s^{-1}	(Brody, 2002, Lavergne & Trissl, 1995)
Rate constant of heat dissipation in core antenna associated with open PSII reaction centers	k^{Uo}_d	0.00 s^{-1}	(Roelofs et al., 1992)
Rate constant of electron transfer from oxygen evolution complex to P_{680}^+	k_z	5×10^6 s^{-1}	(Lazar, 1999)

The number of chlorophylls in the core antenna of an active PSII reaction center	N	70	(Peter & Thornber, 1991)
Temperature	T	298 K	
The peak wavelength of light absorbance of chlorophyll in PSII reaction center	λ_P	680 nm	(Schatz et al., 1988)
The peak wavelength of light absorbance of certain chlorophyll	λ_{abs}	Dependent on the location of the chlorophyll	
The peak wavelength of light absorbance of chlorophyll in core antenna	λ_{Chl}	673 nm	(Schatz et al., 1988)

Table 1 , cont.

* Estimated value based on the rate of excitation energy transfer between chlorophylls.

Table 2

Comparisons of the major assumptions and results of current models of fluorescence induction.

Model	Major Assumptions	Major results and conclusions
Stirbet *et al.* (1998)	The model incorporates reactions at both the acceptor side and the donor sides of photosystem II, and excitation energy quenching by the oxidized plastoquinone molecules from the lipid matrix of the thylakoid membrane. Chlorophyll fluorescence is calculated based on the redox state of Q_A.	The point J corresponds to peak $[Q_A^-Q_B]$, the point I corresponds to peak $[Q_A^-Q_B^-]$, and point P corresponds to peak $[Q_A^-Q_B^{2-}]$.
Lebedeva *et al.* (2002)	This model includes a) a detailed description of reactions related to PSII, PSI, cytochrome b_6f complex, ATP synthesis, and the possible leakage of H^+, K^+, and Cl^- through thylakoid membrane; b) the dependence of electron transfer rate on the membrane potential; c) no molecular mechanism of the oxygen evolution complex.	The model describes FI under different light conditions. Fluorescence at every moment is determined by the sum of fluorescence emission by different fluorescence-emiting PSII states.
Trissl and Lavergne (1995)	The model assumes a) a homogeneous PSII population, b) an exciton-radical pair equilibrium	A simple analytical relation is derived describing fluorescence

	mechanism, c) different rates of exciton transfer between core and peripheral antenna beds, d) a calculation of fluorescence emission based on the amount of excited singlet chlorophyll in both core and peripheral antenna	induction kinetics under the presence of DCMU.

Lazar (2003)	The model a) assumes equilibrium of excited energy among all light harvesting and reaction center pigments, b) assumes reversible radical pair formation mechanism, c) considers both the acceptor side and donor side reactions and PSII heterogeneity, d) calculates chlorophyll fluorescence based on concentrations of different forms of fluorescence-emitting excited state forms.	1) F_o phase is influenced by primary photochemistry of PSII and non-radiative loss of excitation energy, 2) the point J is influenced by P_{680}^+ quenching, changes in the rate constant of electron transfer from Q_A^- to Q_B due to different S states of OEC, 3) the P point is influenced by the state transition of OEC and electron transfer from Q_A^- to Q_B.
Vredenberg (2000)	The model a) categorizes the reaction center into open, semi-open and closed states which can accept 2, 1 and 0 electrons respectively, b) assumes at least two turnovers are required for stationary closure of a reaction center, c) considers the back transfer of excitons from open and semi-open reaction center to antenna, d) does not consider oxygen evolution mechanism, e) does not include reaction mechanisms after Q_A reduction.	Light dependent changes in the rate constant of charge recombination causes changes in F_o. Fluorescence at point J corresponds to accumulation of photosynthetic units in the semi-open state. Fluorescence at point I is interpreted to be of systems with 100% of

		reaction centers closed.
Schreiber and Krieger (1996)	This model a) assumes reversible radical pair mechanism; b) assumes that Q_A reduction stimulates both prompt and recombinant fluorescence with only recombinant fluorescence being in competition with nonradiative energy losses at the reaction center, c) does not include an oxygen evolution mechanism.	Changes in the rate constants of nonradiative energy loss processes in PSII modulate the yield of recombination fluorescence in closed centers, which leads to fluorescence increase after J of FI. The fluorescence emission at the J phase can be purely attributed to prompt fluorescence with high enough rate constants of nonradiative energy loss processes in PSII.
Our model	Our model a) assumes a reversible radical pair model, b) describes the energy transfer between different antenna components, c) considers both the acceptor and donor side electron transfer reactions, d) calculates fluorescence emission based on the amount of excited singlet-state chlorophylls, e) considers the active and inactive PSII centers.	The point J corresponds to the peak $[Q_AQ_B^-]$ and $[Q_A^-Q_B^-]$. The point I corresponds to the first shoulder of the $[Q_A^-Q_B^{2-}]$. The P point corresponds to the peak $[Q_AQ_B^{2-}]$ and $[PQH_2]$. The dip after J phase is closely associated with P_{680}^+ quenching. The relative size of core antenna and

	peripheral antenna influences the F_o level.

Table 2, cont.

Table 3

The origins and major influencing factors of different inflexion points based on this model.

Inflexion point	Origin and major influencing factors
O	Influenced by the relative size of core antenna and peripheral antenna of PSII reaction center. Chlorophylls detached from reaction center contribute to fluorescence emission at O level.
J	Corresponds most closely to the peak concentrations of $Q_AQ_B^-$ and $Q_A^-Q_B^-$.
I	Corresponds most closely to the first shoulder of the concentration change of $Q_A^-Q_B^{2-}$
P	Corresponds most closely to the peak concentrations of $Q_A^-Q_B^{2-}$ and PQH_2.

Appendix I The ordinary differential equations representing the model of fluorescence induction (Fig. 1). This set of equations only includes the differential equations representing the change of concentrations of components associated with active PSII reaction centers. Same set of different equations were used to describe the concentration changes of components associated with inactive PSII reaction centers. The inactive and active reaction centers were assumed to share the same plastoquinol pool. The differential equation for $[PQH_2]$ in the full model combines the contributions from reactions associated with both active and inactive reaction centers. The rate equation for each velocity variable is listed in Appendix II. The abbreviations of reaction velocities used in the system of differential equations are defined in Appendix III.

$$\frac{d[A_p]}{dt} = I_a - v_{Af} - v_{Ad} - v_{AU} + v_{UA} - v_{P680qA} - v_{PQqA}$$

$$\frac{d[U]}{dt} = I_c + v_{AU} - v_{UA} - v_{Uf} - v_{Ud} - v_{P680qU} - v_1 + v_{\_1} - v_{PQqU}$$

$$\frac{d[P_{680}{}^{+}Pheo^{-}]}{dt} = v_1 - v_{-1} - v_{z\_1} - v_{2\_1} + v_{r2\_1}$$

$$\frac{d[P_{680}{}^{+}Pheo]}{dt} = v_{2\_1} - v_{r2\_1} - v_{z\_2}$$

$$\frac{d[P_{680}Pheo^{-}]}{dt} = v_{z\_1} - v_{2\_2} + v_{r2\_2}$$

$$\frac{d[S_{1T}]}{dt} = v_{s0\_s1} - v_{1Z}$$

$$\frac{d[S_{2T}]}{dt} = v_{s1\_s2} - v_{2Z}$$

$$\frac{d[S_{3T}]}{dt} = v_{s2\_s3} - v_{3Z}$$

$$\frac{d[S_{0T}]}{dt} = v_{s3\_s0} - v_{0Z}$$

$$\frac{d[S_{1Tp}]}{dt} = v_{1Z} - v_{s1\_s2}$$

$$\frac{d[S_{2Tp}]}{dt} = v_{2Z} - v_{s2\_s3}$$

$$\frac{d[S_{3Tp}]}{dt} = v_{3Z} - v_{s3\_s0}$$

$$\frac{d[S_{0Tp}]}{dt} = v_{0Z} - v_{s0\_s1}$$

$$\frac{d[Q_A Q_B]}{dt} = v_3 - v_{\_r3} - v_{2\_00\_1} - v_{2\_00\_2} + v_{r2\_00\_1} + v_{r2\_00\_2}$$

$$\frac{d[Q_A^{-} Q_B]}{dt} = v_{2\_00\_1} + v_{2\_00\_2} - v_{r2\_00\_1} - v_{r2\_00\_2} - v_{AB1} + v_{BA1} + v_{3\_n} - v_{\_r3\_n}$$

$$\frac{d[Q_A Q_B^{-}]}{dt} = v_{AB1} - v_{BA1} - v_{2\_01\_1} - v_{2\_01\_2} + v_{r2\_01\_1} + v_{r2\_01\_2}$$

$$\frac{d[Q_A^{-} Q_B^{-}]}{dt} = v_{BA2} - v_{AB2} + v_{2\_01\_1} + v_{2\_01\_2} - v_{r2\_01\_1} - v_{r2\_01\_2}$$

$$\frac{d[Q_A Q_B^{2-}]}{dt} = v_{AB2} - v_{BA2} - v_3 + v_{\_r3} - v_{2\_02\_1} - v_{2\_02\_2} + v_{r2\_02\_1} + v_{r2\_02\_2}$$

$$\frac{d[Q_A^{-} Q_B^{2-}]}{dt} = v_{\_r3\_n} - v_{3\_n} + v_{2\_02\_1} + v_{2\_02\_2} - v_{r2\_02\_1} - v_{r2\_02\_2}$$

$$\frac{d[PQH_2]}{dt} = v_3 + v_{3\_n} - v_{\_r3} - v_{\_r3\_n} - v_{\_pq\_ox}$$

Appendix II. The rate equations describing the reactions associated with active reaction centers used in the model of fluorescence induction. The set of equations for the reactions associated with the inactive reaction centers were similar to this set and not listed. See appendix for definition of abbreviations. The details for derivation of each rate equations are in the main text. The detailed description for each abbreviation was listed in Appendix III except that the rate constants are listed in table 1.

$I_a = 220I_{in}/(290 + 200n + 70x + 220x + 200nx)$

$I_c = 70\ I_{in}/(290 + 200n + 70x + 220x + 200nx)$

$A_i = 220xI_{in}/(290 + 200n + 70x + 220x + 200nx)$

$U_{if} = 35xI_{in}/(290 + 200n + 70x + 220x + 200nx)$

$v_{Af} = [A_p]k^a_f$

$v_{Ad} = [A_p]k^a_d$

$v_{AU} = [A_p]k_{AU}(1 - x/(1+x))$

$v_{UA} = [U]k_{UA}$

$v_{Uf} = [U]k^u_f$

$v_{Ud} = [U](1-q)k^{Uc}_d + [U]qk^{Uo}_d$

where $q = [Q_A]/([Q_A] + [Q_A^-])$

where $[Q_A] = [Q_AQ_B] + [Q_AQ_B^-] + [Q_AQ_B^{2-}]$

$[Q_A^-] = [Q_A^-Q_B] + [Q_A^-Q_B^-] + [Q_A^-Q_B^{2-}]$

$v_1 = q[P_{680}^*Pheo]k^o_1 + [P_{680}^*Pheo](1-q)(1-p)k^c_1 + [P_{680}^*Pheo](1-q)pk^o_1$

where $[P_{680}^*Pheo] = [U][P_{680}Pheo]\,(1+\frac{k_{-t}}{k_t})^{-1}/70$

and $\frac{k_{-t}}{k_t} = \exp[-hc/(kT)(\lambda_{Chl}^{-1} - \lambda_P^{-1})]$

$v_{-1} = q[P_{680}^+Pheo^-]k^o_{-1} + (1-q)[P_{680}^+Pheo^-]k^c_{-1}$

$v_{S1\_S2} = [S_{1Tp}]k_{o12}$

$v_{S2\_S3} = [S_{2Tp}]k_{o23}$

$v_{S3\_S0} = [S_{3Tp}]k_{o30}$

$v_{S0\_S1} = [S_{0Tp}]k_{o01}$

Coeff1 = $[P_{680}^{+}Pheo^{-}]/[P_{680}PheoT]$

Where $[P_{680}PheoT] = [P_{680}Pheo] + [P_{680}^{+}Pheo] + [P_{680}Pheo^{-}] + [P680^{+}Pheo^{-}]$

$v_{1z\_1} = [S_{1T}]k_z Coeff1$

$v_{2z\_1} = [S_{2T}]k_z Coeff1$

$v_{3z\_1} = [S_{3T}]k_z Coeff1$

$v_{0z\_1} = [S_{0T}]k_z Coeff1$

$v_{z\_1} = v_{1z\_1} + v_{2z\_1} + v_{3z\_1} + v_{0z\_1}$

Coeff2 = $[P_{680}^{+}Pheo]/[P_{680}PheoT]$

$v_{1z\_2} = [S_{1T}]k_z Coeff2$

$v_{2z\_2} = [S_{2T}]k_z Coeff2$

$v_{3z\_2} = [S_{3T}]k_z Coeff2$

$v_{0z\_2} = [S_{0T}]k_z Coeff2$

$v_{z\_2} = v_{1z\_2} + v_{2z\_2} + v_{3z\_2} + v_{0z\_2}$

$v_{1z} = v_{1z\_1} + v_{1z\_2}$

$v_{2z} = v_{2z\_1} + v_{2z\_2}$

$v_{3z} = v_{3z\_1} + v_{3z\_2}$

$v_{0z} = v_{0z\_1} + v_{0z\_2}$

$v_{AB1} = [Q_A^{-}Q_B]k_{AB1}$

$v_{BA1} = [Q_AQ_B^{-}]k_{BA1}$

$v_{AB2} = [Q_A^{-}Q_B^{-}]k_{AB2}$

$v_{BA2} = [Q_AQ_B^{-2}]k_{BA2}$

[PQT] = 6

$v_3 = [Q_AQ_B^{2-}]k_3[PQ]/[PQT]$

$v_{r3} = [Q_AQ_B]k_{r3}[PQH_2]/[PQT]$

$v_{3\_n} = [Q_A^{-}Q_B^{2-}]k_3[PQ]/[PQT]$

$v_{r3\_n} = [Q_A^{-}Q_B]k_{r3}[PQH_2]/[PQT]$

$v_{pq\_ox} = [PQH_2]k_{ox}$

$v_{2\_1} = [P680^{+}Pheo^{-}]k_2q$

$v_{2\_2} = [P680Pheo^{-}]k_2q$

$a = [Q_AQ_B]/([Q_AQ_B] + [Q_AQ_B^{-}] + [Q_AQ_B^{2-}])$

$b = [Q_AQ_B^{-}]/([Q_AQ_B]+[Q_AQ_B^{-}] + [Q_AQ_B^{2-}])$

$c = [Q_A Q_B^{2-}]/([Q_A Q_B]+[Q_A Q_B^{-}] + [Q_A Q_B^{2-}])$

$v_{2\_00\_1} = v_{2\_1}a$

$v_{2\_01\_1} = v_{2\_1}b$

$v_{2\_02\_1} = v_{2\_1}c$

$v_{2\_00\_2} = v_{2\_2}a$

$v_{2\_01\_2} = v_{2\_2}b$

$v_{2\_02\_2} = v_{2\_2}c$

$CE_1 = [P_{680}^{+}Pheo]/[P_{680}PheoT]$

$v_{r2\_00\_1} = CE_1[Q_A^{-}Q_B]k_2/Ke$

$v_{r2\_01\_1} = CE_1[Q_A^{-}Q_B^{-}]k_2/Ke$

$v_{r2\_02\_1} = CE_1[Q_A^{-}Q_B^{-2}]k_2/Ke$

$v_{r2\_1} = v_{r2\_00\_1} + v_{r2\_01\_1} + v_{r2\_02\_1}$

$CE_2 = [P_{680}Pheo]/[P_{680}PheoT]$

$v_{r2\_00\_2} = CE_2[Q_A^{-}Q_B]k_2/Ke$

$v_{r2\_01\_2} = CE_2[Q_A^{-}Q_B^{-}]k_2/Ke$

$v_{r2\_02\_2} = CE_2[Q_A^{-}Q_B^{-2}] \times k_2/Ke$

$v_{r2\_2} = v_{r2\_00\_2} + v_{r2\_01\_2} + v_{r2\_02\_2}$

$v_{P680qU} = [U]([P_{680}^{+}Pheo] + [P_{680}^{+}Pheo^{-}])k_c$

$v_{P680qA} = [A]([P_{680}^{+}Pheo] + [P_{680}^{+}Pheo^{-}])k_c$

$k_q = 0.15(k_f + k_h)/ [PQT]$

$v_{PQqU} = [U][PQ]k_q$

$v_{PQqA} = [A][PQ]k_q$

$\Phi_f = k^a_f A_p + ([U]+[U_i])k^u_f + k^a_f[A_{ip}] + k^u_f[U_{ifc}]$

Appendix III Definitions of all abbreviations except rate constants used in the model.

Abbrev.	Description	Unit
$[A_p]$	Concentration of excitation energy on peripheral antenna of photosystem II	μmol m^{-2}
$[P_{680}{}^{*}Pheo]$	The concentration of excited P_{680} associated with Pheo	μmol m^{-2}
$[P_{680}{}^{+}Pheo]$	The concentration of $P_{680}{}^{+}$ associated with Pheo	μmol m^{-2}
$[P_{680}{}^{+}Pheo^{-}]$	The concentration of $P_{680}{}^{+}$ associated with $Pheo^{-}$	μmol m^{-2}
$[P_{680}Pheo]$	The concentration of P_{680} associated with Pheo	μmol m^{-2}
$[P_{680}Pheo^{-}]$	The concentration of P_{680} associated with $Pheo^{-}$	μmol m^{-2}
$[P_{680}PheoT]$	The total concentration of $P_{680}Pheo$, $P_{680}{}^{+}Pheo$, $P_{680}Pheo^{-}$ and $P_{680}{}^{+}Pheo^{-}$.	μmol m^{-2}
[PQ]	The concentration of plastoquinone	μmol m^{-2}
[PQ]	The concentration of oxidized plastoquinone	μmol m^{-2}
$[PQH_2]$	The concentration of fully reduced plastoquinone	μmol m^{-2}

[PQT]	The total concentration of plastoquinone and plastoquinol in thylakoid membrane	μmol m^{-2}
$[Q_A]$	The concentration of oxidized Q_A	μmol m^{-2}
$[Q_A^-]$	The concentration of reduced Q_A	μmol m^{-2}
$[Q_AQ_B]$	The concentration of oxidized Q_A associated with oxidized Q_B	μmol m^{-2}
$[Q_A^-Q_B]$	The concentration of reduced Q_A associated with oxidized Q_B	μmol m^{-2}
$[Q_A^-Q_B]$	The concentration of reduced Q_A associated with Q_B^-	μmol m^{-2}
$[Q_A^-Q_B]$	The concentration of reduced Q_A associated with Q_B^{2-}	μmol m^{-2}
$[Q_AQ_B^-]$	The concentration of oxidized Q_A associated with Q_B^-	μmol m^{-2}
$[Q_AQ_B^{2-}]$	The concentration of oxidized Q_A associated with Q_B^{2-}	μmol m^{-2}
$[S_n]$	The concentration of oxygen evolving complex at S_n state	μmol m^{-2}
$[S_{nT}]$	The concentration of oxygen evolving complex at S_n state before donating electron	μmol m^{-2}

	to tyrosine (Y_z)	
$[S_{nTp}]$	The concentration of oxygen evolving complex at S_n state after donating electron to tyrosine (Y_z)	μmol m^{-2}
[U]	Concentration of excitation energy on core antenna of active photosystem II	μmol m^{-2}
$[U_i]$	Concentration of excitation energy on core antenna of inactive photosystem II	μmol m^{-2}
$[U_{ifc}]$	The concentration of excitation energy on chlorophylls detached from core antenna of inactive photosystem II	μmol m^{-2}
$[Y_Z]$	The concentration of primary electron donor for reaction center of PSII (P_{680})	μmol m^{-2}
A_i	Incident photon flux density on peripheral antenna of inactive photosystem II	μmol m^{-2} s^{-1}
A_{iP}	The concentration of excitation energy on peripheral antenna of inactive photosystem II	μmol m^{-2}
I_a	The incident photon flux density on peripheral PSII antenna	μmol m^{-2} s^{-1}
I_c	The incident photon flux density on core antenna of active reaction center	μmol m^{-2} s^{-1}

I_{in}	The total incident photon flux density	μmol m^{-2} s^{-1}
n	The ratio of PSI to PSII	NA
P_{680}	The reaction center chlorophyll of PSII. It can exist in native state (P_{680}), excited state (P_{680}^{*}), or oxidized state (P_{680}^{+}).	NA
Pheo	Pheophytin, the first electron acceptor of primary charge separation in PSII. It can exist in either native state (Pheo) or reduced state ($Pheo^{-}$).	NA
q	The proportion of oxidized Q_A	NA
Q_A	The first quinine electron acceptor of PSII	NA
Q_B	The second quinine electron acceptor of PSII	NA
U_{if}	Incident photon flux density on chlorophylls detached from core antenna of inactive photosystem II	μmol m^{-2} s^{-1}
$v_{\_pq\_ox}$	The rate of PQH_2 oxidation by cyt b_6f	μmol m^{-2} s^{-1}
$v_{\_r3}$	The rate of the exchange of PQH_2 with Q_B associated with Q_A	μmol m^{-2} s^{-1}
$v_{\_r3\_n}$	The rate of exchange of PQH_2 with Q_B	μmol m^{-2} s^{-1}

	associated with Q_A^-	
v_1	The rate of charge separation in the active PSII reaction center	μmol m^{-2} s^{-1}
v_{-1}	The rate of charge recombination in the active PSII reaction center	μmol m^{-2} s^{-1}
$v_{2\_0m\_n}$	The rate of reactions relating to electron transfer from $Pheo^-$ to Q_A where m represents the redox state of Q_B with 0 for Q_B, 1 for Q_B^- and 2 for Q_B^{-2}, and n represents the redox state of P_{680} with 1 for P_{680}^+ and 2 for P_{680}, e.g. $v_{2\_00\_1}$: the rate of reduction of Q_AQ_B by $P_{680}^+Pheo^-$	μmol m^{-2} s^{-1}
v_{2_1}	The rate of Q_A reduction by $P_{680}^+Pheo^-$	μmol m^{-2} s^{-1}
v_{2_2}	The rate of Q_A reduction by $P_{680}Pheo^-$	μmol m^{-2} s^{-1}
v_3	The rate of exchange of PQ with Q_B^{2-} associated with Q_A	μmol m^{-2} s^{-1}
v_{3_n}	The rate of exchange of PQ with Q_B^{2-} associated with Q_A^-	μmol m^{-2} s^{-1}
v_{AB1}	The rate of electron transfer from Q_A^- to Q_B	μmol m^{-2} s^{-1}
v_{AB2}	The rate of electron transfer from Q_A^- to Q_B^-	μmol m^{-2} s^{-1}

v_{Ad}	The rate of heat dissipation from the peripheral antenna	μmol m^{-2} s^{-1}
v_{Af}	The rate of fluorescence emission from the peripheral antenna	μmol m^{-2} s^{-1}
v_{AU}	The rate of excitation energy transfer from peripheral to core antenna	μmol m^{-2} s^{-1}
v_{BA1}	The rate of electron transfer from Q_B^- to Q_A	μmol m^{-2} s^{-1}
v_{BA2}	The rate of electron transfer from Q_B^{-2} to Q_A	μmol m^{-2} s^{-1}
v_{nz}	The rate of oxidation of S_n state of oxygen evolution complex	μmol m^{-2} s^{-1}
v_{nz_1}	The rate of electron transfer from oxygen evolution complex at S_n state to P_{680}^+ associated with $Pheo^-$ via Y_z	μmol m^{-2} s^{-1}
v_{nz_2}	The rate of electron transfer from oxygen evolution complex at S_n state to P_{680}^+ associated with Pheo via Y_z	μmol m^{-2} s^{-1}
v_{P680qA}	The rate of quenching of excitation energy in the peripheral antenna by P_{680}^+	μmol m^{-2} s^{-1}
v_{P680qU}	The rate of quenching of excitation energy in the core antenna by P_{680}^+	μmol m^{-2} s^{-1}
v_{PQqA}		μmol m^{-2} s^{-1}

	The rate of quenching of excitation energy in the peripheral antenna by oxidized plastoquinone	
v_{PQqU}	The rate of quenching of excitation energy in the core antenna by oxidized plastoquinone	μmol m^{-2} s^{-1}
$v_{r2\_0m\_n}$	The back reaction of $v_{2\_0m\_n}$, see $v_{2\_0m\_n}$ for details	μmol m^{-2} s^{-1}
v_{r2_1}	The rate of Q_A^- oxidation by P_{680}^+Pheo	μmol m^{-2} s^{-1}
v_{r2_2}	The rate of Q_A^- oxidation by P_{680}Pheo	μmol m^{-2} s^{-1}
v_{sm_sn}	The rate of transition from S_m state to S_n state of oxygen evolution complex	μmol m^{-2} s^{-1}
v_{UA}	The rate of excitation energy transfer from core antenna to peripheral antenna	μmol m^{-2} s^{-1}
v_{Ud}	The rate of heat dissipation of excitation energy from the core antenna of active PSII reaction center	μmol m^{-2} s^{-1}
v_{Uf}	The rate of fluorescence emission from the core antenna of active reaction center	μmol m^{-2} s^{-1}
v_{z_1}	The rate of P_{680}^+Pheo$^-$ reduction	μmol m^{-2} s^{-1}
v_{z_2}	The rate of P_{680}^+Pheo reduction	μmol m^{-2} s^{-1}

x	The ratio of the concentration of inactive PSII reaction center to that of active reaction center	NA
Φ_f	Fluorescence yield	μmol m^{-2} s^{-1}